




Cite this: *Phys. Chem. Chem. Phys.*,  
2017, **19**, 22282

# A simplified *ab initio* treatment of diradicaloid structures produced from stretching and breaking chemical bonds

Suvonil Sinha Ray,<sup>a</sup> Anirban Ghosh,<sup>a</sup> Anindita Shit,<sup>b</sup> Rajat K. Chaudhuri<sup>c</sup> and Sudip Chattopadhyay \*<sup>a</sup>

The present investigation reports on the prospect of using state specific multireference perturbation theory (SSMRPT) with an improved virtual orbital complete active space configuration interaction (IVO-CASCI) reference function (IVO-SSMRPT) to generate potential energy surfaces (PESs) for molecular systems [such as CH<sub>4</sub>, C<sub>2</sub>H<sub>6</sub>, C<sub>2</sub>H<sub>4</sub>, H<sub>2</sub>O<sub>2</sub>, LiH, and KN] by stretching and breaking of suitable bonds with modest basis sets. We have also revisited the dissociation energy profile of triplet ketene which exhibits a step-like structure in the observed rate. The application of the method has also been made to the ionization energies of H<sub>2</sub>O. Although the perturbative corrections are obtained by the diagonalization of the effective Hamiltonian, in IVO-SSMRPT, only one physically relevant solution is achievable. It is parameter free and does not require any threshold to avoid the intruder problem. It is strictly size-extensive and size-consistent provided that local orbitals are used. The PESs obtained with our approach are smooth all along the reaction path. Our estimates are in close agreement with the available reference data indicating that IVO-SSMRPT is a robust paradigm for the accurate computation of ground, excited and ionized states as it captures the mutual inter-play of different flavors of correlation effects in a balanced and accurate way.

Received 26th May 2017,  
Accepted 31st July 2017

DOI: 10.1039/c7cp03564k

rsc.li/pccp

## 1. Introduction

Despite the various theoretical developments and subsequent numerical implementations, correctly characterizing the electronic structure properties of systems that simultaneously display chemically relevant static (associated with the configurational quasidegeneracy or rearrangement of electrons within partially filled shells) and dynamical (due to the instantaneous scattering of electrons at short distances) electron correlation still provides methodological challenges in the realm of quantum chemistry.<sup>1,2</sup> It is now well accepted that to describe molecules with stretched or broken bonds, or systems with partially occupied near-degenerated orbitals, the method used should be sufficiently flexible to accurately model the intricate inter-play of both correlation effects. Generally, along the bond dissociation (or formation) energy profiles (termed as the potential energy surface, PES) of ground, excited, and ionized states, the character of the wave functions of interest changes very rapidly. For studying such cases, multireference (MR) wave functions are

needed to provide even a qualitatively correct description since two or more configurations are required to furnish a proper zeroth-order description of the state(s). Although in such situations, conventional single-reference (SR) methods often fail to bestow a meaningful estimate (owing to the helplessness of a single-determinant reference function to appropriately describe the zeroth-order wave function), attempts at alleviating the problems have already been undertaken by various works using suitably modified SR ansatz.<sup>3–8</sup> From our point of view, an MR protocol has more flexibility compared to such SR-based theoretical models.

Multireference perturbation theory (MRPT) is one of the simple and popular quantum chemical tools for the treatment of a variety of strongly correlated systems.<sup>9–31</sup> A number of MRPTs have been designed and implemented over the decades (each of the methods has its own merits and demerits<sup>1,2,32</sup>), among which the state specific MRPT (SSMRPT) method<sup>2,17,18</sup> with a complete active space self-consistent field (CASSCF) reference function<sup>33</sup> is growing in popularity as it has been successfully employed to describe homolytic bond breaking/formation, and transition states of chemical reactions where traditionally, the effective Hamiltonian-based MR methods are plagued by intruders (raised when the zeroth-order energy of the reference and excited configurations are near-degenerate).<sup>34</sup> The highly nonlinear nature of the orbital optimization step in

<sup>a</sup> Department of Chemistry, Indian Institute of Engineering Science and Technology, Shibpur, Howrah 711103, India. E-mail: sudip@chem.iests.ac.in

<sup>b</sup> Department of Chemistry, Kandi Raj College, Kandi, Murshidabad 742137, India

<sup>c</sup> Indian Institute of Astrophysics, Bangalore 560034, India

CASSCF calculation can lead to multiple solutions in conjunction with the convergence difficulties which makes the CASSCF-SSMRPT protocol less effective when dealing with large molecules. Recently we published a new protocol, called IVO-SSMRPT,<sup>30</sup> which has been developed in a way to combine the strengths of (i) the IVO-CASCI (improved virtual orbital complete active space configuration interaction)<sup>35</sup> and (ii) the SSMRPT methods.<sup>17</sup> Here, IVO-CASCI is employed for the zeroth-order description of the MR problem (suited for covering the dominant part of the static electron correlation). Given a IVO-CASCI wave function, the missing dynamical electron correlation effects in the treatment of IVO-CASCI can be efficiently recovered using SSMRPT. The main objective of this method is to lower the cost of treating quasidegenerate situations with large reference spaces with a moderate and controllable accuracy. The worthiness of employing the IVO-CASCI in lieu of CASSCF lies in the fact that the former does not need iterations, nor does it face convergence problems as it avoids the orbital optimization step altogether in conjunction with retaining all the merits of the CASSCF scheme. The IVO-CASCI method is less susceptible to multiple solutions than CASSCF and it is computationally less laborious for small- to medium-sized active spaces. Although the orbitals are determined using single-reference means in IVO-CASCI, this scheme allows multiple electronic states to be treated on an equal footing to describe the intersections of those states. As a result, IVO-CASCI can be used as a workhorse for the study of chemical processes and situations displaying quasidegeneracies.<sup>35</sup> The IVO-SSMRPT method has all the marks of an effective computational method: (i) rigorous size extensivity and size-consistency with localized orbitals, (ii) robustness against the intruder problem without any *ad hoc* level shift<sup>36</sup> as the zero-order energies corresponding to the virtual functions are well separated from the zero-order energy of the state being considered, and consequently circumventing divergences in the perturbation summation, (iii) the IVO-SSMRPT method used here is inherently spin-free as the first-order correction to the wavefunction is an eigenfunction of the spin operators, thereby circumventing the spin contamination issue and hence it is capable of treating the electronic wave function of closed- and open-shell states accurately, (iv) excited electronic states can be dealt with at the same level of accuracy as the ground state as long as the zero-order energy is well-separated from the energies of the virtual functions, (v) IVO-SSMRPT coincides with the corresponding single-reference perturbation theory in the case of a HF wave function, and (vi) the model space components in IVO-SSMRPT can be either adjusted or fixed at the IVO-CASCI values during the estimations of dynamical correlation. These properties indicate that IVO-SSMRPT is a serious candidate when an MR problem needs to be solved. Note that the recent works reported in the literature indicate that accurate MRPT values can be obtained without fully optimized CASSCF orbitals.<sup>20,21,23</sup> This bodes well for a SSMRPT based on IVO-CASCI. Despite their success in the description of electronic structure of chemical systems (of varying complexity) plagued by quasidegeneracy to different extents, the widely used MRPT methods such as MRMP2 [second-order Møller–Plesset (MP) perturbation theory],<sup>9</sup> CASPT2 (second-order complete active space

perturbation theory)<sup>11</sup> and GVVPT2 (second-order generalized Van-Vleck PT)<sup>16</sup> have some crucial limitations.<sup>36–38</sup> Perhaps the notable unsettling features of these methods are the intruder state problem and the lack of size-extensivity. Although the former problem can be tackled by the level (denominator) shift technique,<sup>36,37</sup> it introduces some arbitrariness in the estimated values. Moreover, in investigations of multiple excited states, finding a ubiquitous level shift for all the states under consideration appears to be a challenging task.<sup>37</sup>

Here, we study (i) C–H bond-breaking in CH<sub>4</sub>, (ii) C–C bond breaking in C<sub>2</sub>H<sub>6</sub>, (iii) O–O bond breaking in H<sub>2</sub>O<sub>2</sub>, (iv) C=C bond dissociation in C<sub>2</sub>H<sub>4</sub>, (v) dissociation of triplet (T<sub>1</sub>) ketene into triplet carbene (<sup>3</sup>CH<sub>2</sub>) and CO, (vi) low-lying excited states of LiH and KN, and (v) vertical ionization energies of H<sub>2</sub>O to assess the accuracy and generality of the IVO-SSMRPT method and compare its performance with that of the other established methods available in the literature. The published theoretical data of the experimentally unknown KN is very limited<sup>39</sup> and thus, a comprehensive theoretical investigation would be very useful to identify its structural properties experimentally. We want to mention that the ability to remove the pervasive problem of intruder states to yield the target wavefunction preferentially in a size-extensive fashion may enable many formally demanding problems to be correctly described within what is an operationally state-universal approach, benefiting from its ease of use.

## II. Theoretical background: a Hilbert space fully relaxed single root MRPT with IVOs

The present paper deals with an MRPT developed at the (pseudo) second order level, based on a multiexponential Jeziorski–Monkhorst (JM) expansion using individual reference functions as perturbers. Thanks to this nature of the JM perturbers, an effective Hamiltonian may be constructed that allows for the dressing of the Hamiltonian matrix within the reference space formed from a IVO-CASCI and accounts for the coupling between the static and dynamic correlation effects by state specific parametrization of JM ansatz using the SSMRPT protocol.<sup>30</sup> The SSMRPT method has a solid theoretical background as the full-blown SSMR coupled cluster (CC), the SSMRCC method<sup>40</sup> is foundational to the emergence of the SSMRPT approach (by the quasi-linearization of cluster finding equation) without significantly sacrificing the accuracy of the parent method. In the SSMRPT method, parametrization of the target state is described as:  $|\psi\rangle = \sum_{\mu} \exp(T_{\mu})|\phi_{\mu}\rangle c_{\mu}$  where a separate cluster-operator  $T_{\mu}$  is associated with each reference function  $\phi_{\mu}$  needed to build a correct zeroth-order approximation,  $\psi [= \sum_{\mu} |\phi_{\mu}\rangle c_{\mu}]$  where each  $\phi_{\mu}$  is weighted by the coefficient]. For convenience, we assume that the set of  $\{\phi_{\mu}\}$  form a complete active or model space (CAS/CMS). The reference coefficients  $c_{\mu}$ s and  $T_{\mu}$ s are not known a priori. Here, initial coefficients ( $c_{\mu}^0$ ) and the orbitals are determined by IVO-CASCI calculation, which can be state-specific.

Generally all genuine MR methods need a manual selection of the CAS/CMS (that is spanned by relevant configuration) for the problem of interest, the selection of which generally needs insights into the chemical nature of the system under consideration. The nature of the CAS/CMS can affect the accuracy and the convergence of the calculations.

In the SSMRPT method, the JM ansatz is inserted into the Schrödinger equation:

$$H \sum_{\mu} \exp(T_{\mu}) |\phi_{\mu}\rangle c_{\mu} = E \sum_{\mu} \exp(T_{\mu}) |\phi_{\mu}\rangle c_{\mu} \quad (1)$$

and the Schrödinger equation is converted into an effective eigenvalue problem which yields the energy of the target state (and the expansion coefficients):

$$\sum_{\nu} \tilde{H}_{\mu\nu}^{(2)} c_{\nu} = E^{(2)} c_{\mu} \quad (2)$$

with  $\tilde{H}_{\mu\nu}^{(2)} = H_{\mu\nu} + \sum_l H_{\mu l} t_{\nu}^{(1)}(\nu)$  as a reference-specific similarity transformed Hamiltonian and it contains connected terms for CAS/CMS. In the Rayleigh–Schrödinger variant of the SSMRPT formalism, a set of (first-order) amplitude equations (rather than projection equations) may be expressed in a more compact form (which produces a sufficient number of equations to determine the amplitudes):

$$t_{\mu}^{(1)}(\mu) = \frac{H_{l\mu} + \sum_{\nu}^{\nu \neq \mu} t_{\nu}^{(1)}(\nu) H_{\mu\nu} (c_{\nu}^0 / c_{\mu}^0)}{(E_{\text{CAS}} - H_{\mu\mu}) + (E_{0,\mu\mu} - E_{0,l})} \quad (3)$$

where  $t_{\mu}^{(1)}(\nu) = \langle \chi_{\nu}^{\mu} | T_{\nu}^{(1)} | \phi_{\mu} \rangle$ ,  $\langle \phi_{\mu} | H | \phi_{\nu} \rangle = H_{\mu\nu}$ , and  $\langle \chi_{\nu}^{\mu} | H | \phi_{\mu} \rangle = H_{l\mu}$ . Appearance of the second term, usually called the renormalization term (couples the cluster amplitudes of various functions) is primarily responsible for the rigorous size-extensivity and intruder free nature of the method.  $E_0$  can be characterized as the expectation value of  $H_0$  with respect to a specific configuration. It is important to note that in the SSMRPT computations, only those cluster amplitudes are coupled together in the working equations which share a common set of orbitals. Therefore, the leading computational cost is not very significant. One issue that deserves attention is the question of freedom from singularities (due to the intruder states) of our method. The denominator in eqn (3) is never divergent as long as the zeroth-order energy of the target state is well-separated from the energies of the virtual functions. This is due to the fact that the denominator of the amplitude finding equation is dominated by  $[E_{\text{CAS}} - E_{0,l}]$ , since  $[E_{0,\mu\mu} - H_{\mu\mu}]$  is much smaller than any of the individual terms constituting the difference. So long as  $E_{\text{CAS}}$  is well apart from  $E_{0,l}$  (either virtual orbital energies or the energies of the virtual determinants), the theory avoids the intruder state problem in a natural manner, without having to add an arbitrary shift in the denominator. While this is likely to be the situation for the ground state and a few low-lying excited states, intruders are more likely to appear if one tries to focus the energy of a rather high-lying state. It should be noted that eqn (3) contains the coefficient,  $c_{\mu}$  for the target state indicating the state specificity of the method. Consequently, only one eigenvalue

corresponding to the state of interest is a physically acceptable solution, although the effective Hamiltonian defined within the entire CAS provides as many eigenvalues as the dimension of the model space during diagonalizing. Apart from the target root, other roots serve for “buffering” and getting rid of the intruder states by shifting them away. The requirement to solve for various states at a time is lifted in our state specific theory. Note that the amplitude equations consist of two terms, *viz.* single-reference and a renormalization or coupling part and thus they reduce to the corresponding SR perturbation theory, in the case of a one-dimensional reference space. We wish to stress here that supplementary sufficiency conditions have to be included to filter the redundancy in the JM-ansatz based SSMR methods and thereby generate the appropriate amplitude equations starting from the Schrödinger equation, eqn (1).<sup>2,17</sup> As eqn (3) holds for each  $\mu$  and  $l$ , the number of cluster finding equations is congruous if employing as many  $\chi$ s for a given  $\phi_{\mu}$  as the number of parameters in the specific cluster operator,  $T_{\mu}$ . Although zero-order expansion coefficients ( $c_{\nu}^0$ ) are used to compute the cluster operators in, eqn (3) the IVO-SSMRPT formulation provides a completely relaxed form of target wavefunction as is evident from eqn (2). This offers full flexibility in the treatment of the feed-back effect of the post-IVO-CASCI correlation on the model space component of the wave function in the correlation treatment during the diagonalization process of the effective Hamiltonian operator within the CAS. One can use the unrelaxed version to offer the energy as an expectation value of the effective Hamiltonian operator. Note that if the method does not allow relaxation of the reference coefficients in the correlation calculation, a correct description of the “mixed electronic states” and of the real or avoided curve crossings cannot be expected. We provide here the relaxed results. Note that most single-root MRPT methods, including MRMP2,<sup>9</sup> CASPT2<sup>11</sup> and NEVPT2 (second-order  $n$ -electron valence state perturbation theory),<sup>13</sup> do not account for the relaxation effects of the reference function with the exception of GVVPT2<sup>16</sup> and MCPT2 (second-order multiconfiguration perturbation theory).<sup>15</sup>

Here,  $H_0$  (mono-electronic in nature) can be expressed as  $H_0^{\mu} = \sum_i f_{\mu}^{ii} \{E_i^i\}$  (built by MP multipartitioning scheme),<sup>17,18</sup> with

$$f_{\mu} = \sum_{ij} \left[ f_{ij}^{ij} + \sum_u \left( V_{iu}^{ju} - \frac{1}{2} V_{iu}^{uj} \right) D_{iu}^{\mu} \right] \{E_i^j\} \quad (4)$$

with  $u$  standing both for a doubly and a singly occupied active orbital in  $\phi_{\mu}$  and  $D^{\mu}$ s are the densities characterized by the active orbitals.  $E_i^j$  is a unitary group generator (excitation operator). As the SSMRPT has emerged from quasi-linearization of the full-blown SSMRCC,<sup>40</sup> it offers a clear path forward for improvements. We note that other more sophisticated zeroth-order Hamiltonians such as the one proposed by Dyall<sup>41</sup> can also be straightforwardly applied to the IVO-SSMRPT method.

### III. Numerical results

The present section spells out the numerical results obtained for the energy profiles and electronic structure properties of

spectroscopic interest for various systems with significant diradical/MR character using the IVO-SSMRPT method. Our results have been calibrated against the current generation *ab initio*-approach which is a powerful and versatile tool that allows one to handle various MR-systems. It is very difficult to make a quantitative comparison between these methods because of the use of different basis sets and CAS. Actually, we want to explore the usefulness of our method in terms of its predictive power *vis-a-vis* other standard and established methods in routine use. Note that one of the main ethos of the MR-based calculations is to use as small an active space as possible. The basic requirement of MRPT approaches is that the reference or model space provides a good zero-order description of the target state(s). Keeping in mind the size of the basis sets used here, additionally, we compare the IVO-SSMRPT results to the experimental data which allows us to get better statistics for the performance of our method. The IVO-SSMRPT calculations have been carried out using our own code that interfaces with the GAMESS (General Atomic and Molecular Electronic Structure System) suite of programs<sup>42</sup> and takes advantage of the procedures of the package. The basis sets used here were taken from the EMSL database.<sup>43</sup>

### A. Single-bond breaking

We first present the results obtained with the IVO-SSMRPT method for the biradicals which are intermediate species along the bond dissociation coordinates for breaking the C–H bond in CH<sub>4</sub>, the O–O bond in H<sub>2</sub>O<sub>2</sub>, and the C–C bond in C<sub>2</sub>H<sub>6</sub>. Here, only the C–H, C–C, and O–O bond lengths are changed, while the other degrees of freedom are kept fixed which are taken from the database geometries of CH<sub>4</sub>, C<sub>2</sub>H<sub>6</sub> and H<sub>2</sub>O<sub>2</sub>, respectively.

#### 1. C–H bond-breaking in ground singlet state methane, CH<sub>4</sub>.

We first turn our attention to the C–H bond dissociation in the prototypical ground state ( $X^1A_1$ ) CH<sub>4</sub> molecule, which has been studied by various researchers with different *ab initio* methods<sup>44–50</sup> as an energy surface for the reaction CH<sub>4</sub> → CH<sub>3</sub>• + H• appears as a convenient prototype reaction for the decomposition of alkanes and for the recombination of alkyl radicals. In the calculations, we use the 6-31G\* [*aka.* 6-31G(d)] basis set because various benchmark studies using several single and MR methods including full CI (FCI)<sup>45</sup> have been reported with this basis set which can be used as a gauge to our estimates. Note that the C–H bond breaking in methane leads to a hydrogen radical and a localized methyl radical. Two different geometries are used for the CH<sub>3</sub> moiety. The first geometry is tetrahedral methane (taken from ref. 45) with the 6-31G\* basis set. In the second set of calculations, we follow the scheme of Krylov and coworkers<sup>46</sup> for the large aug-cc-pVTZ basis where a planar CH<sub>3</sub> radical is bonded to a hydrogen atom in such way that the C–H bond remains perpendicular to the plane of the radical. This geometry bears close kinship with the structure of the intermediate generated during the dissociation process of the system, which is pertinent for the kinetics modeling. As in previous work,<sup>45,46,48</sup> the frozen-core approximation is also used here.

The wavefunction of methane starts off being mainly a single closed-shell configuration near the equilibrium region, and then

gradually switches to the description of two dominant configurations in the range 1.5–4.0 Å. The C–H bond breaking in the  $X^1A_1$  CH<sub>4</sub> state may be more appropriately characterized by the two-configuration wave function:  $(\text{core})^2(\sigma_{\text{CH}})^6(\sigma_{\text{CH}'})^2(\sigma_{\text{CH}'^*})^0 - \gamma(\text{core})^2(\sigma_{\text{CH}})^6(\sigma_{\text{CH}'})^0(\sigma_{\text{CH}'^*})^2$ , where the weight of the coefficient  $\gamma$  depends on the C–H bond length – it is large around the equilibrium zone and decreases at stretched bonds. We have used CAS(2,2) in our calculations.

Fig. 1 describes the dissociation energy profile for the  $X^1A_1$  CH<sub>4</sub> molecule with 6-31G\*, obtained by changing the distance of a single C–H bond from 0.8 to 4.6 Å, while the remaining three C–H bonds are fixed to the equilibrium value, 1.086 Å, and the  $\angle$  H–C–H angles are kept fixed at 109.47°. Fig. 2 illustrates the error surfaces against the FCI values for the CH<sub>4</sub>/6-31G\* system as a function of a single C–H bond length. NPEs (nonparallelity errors) for various correlation methods with the 6-31G\* basis set are assembled in Table 1. The problem with the accurate description of the CH PES in CH<sub>4</sub> lies in the intermediate region where the C–H distance is between 2.0 and 3.0 Å as is evident from the previous work using MBPT(4) [four-order many-body perturbation theory].<sup>52</sup> The MBPT(4) level of computation exhibited that the potential rises too sharply in the 2.0–3.0 Å zones of the C–H bond dissociation surface. The SSMRPT method with CASCF and IVO-CASCI orbitals provides a topologically correct description of the C–H bond dissociation potential in all regions of the surface similar to that of the GVVPT2 computations with CAS(8,9).<sup>47</sup> From Fig. 1, it is found that SSMRPT, and SSMRCCSD methods with the smallest active space describe qualitatively the correct shape of the FCI PES. The performance of the CCSD, OD (orbital optimized CC doubles) and CCSD(T) [CC with singles, doubles and non-iterative triples] methods goes down while elongating the C–H bond beyond the equilibrium zone, yielding NPEs around 10 kcal mol<sup>−1</sup>.<sup>48</sup> The UCC and  $\Lambda$  modified CC as well as OD methods considerably improve the performance of the CC and provide NPEs of 2–6 kcal mol<sup>−1</sup>.<sup>45,48</sup> As can be seen from Fig. 2, the IVO-SSMRPT, and CASSCF-SSMRPT errors do

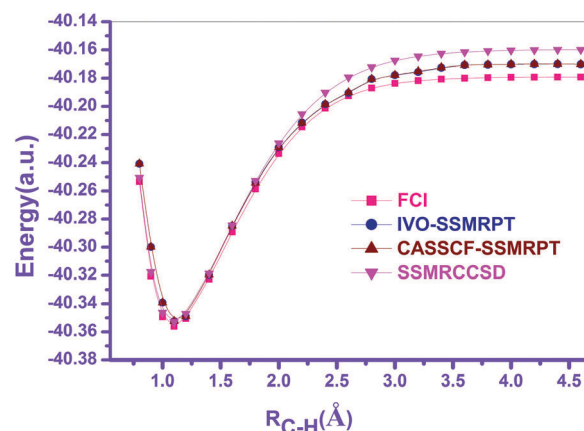


Fig. 1 Plot of the energies of IVO-SSMRPT(2,2), and other methods including FCI (Dutta and Sherrill<sup>45</sup>) against one C–H bond length,  $R_{\text{C-H}}$  (angstrom) for tetrahedral methane (where the other three bonds are kept frozen at 1.086 Å) with the 6-31G\* basis set and one frozen core orbital.

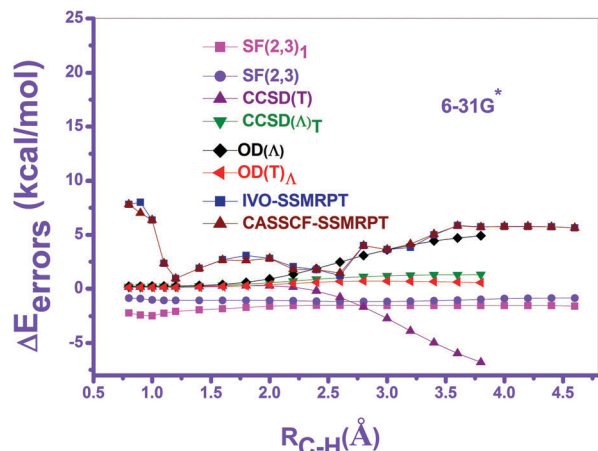


Fig. 2 Errors  $\Delta E$  (in mHartree) from FCI values (Dutta and Sherrill<sup>45</sup>) for the IVO-SSMRPT method along with other selected advanced *ab initio* methods using the 6-31G\* basis set along the C–H bond-breaking coordinate for tetrahedral methane (where the other three bonds are frozen at 1.086 Å).

Table 1 Nonparallelity errors (kcal mol<sup>-1</sup>) relative to FCI for the PESs for selected methods with the 6-31G\* basis set for the dissociation of the C–H bond in methane

Ref.	Method	NPE
Present	IVO-SSMRPT	6.6
	CASSCF-SSMRPT	6.4
45	CASSCF(2,2)	8.69
	CASPT2(4,4)	1.56
	CASPT2(2,2)	1.17
	UCCSD	5.1
	UCCSD(T)	3.2
46	EOM-SF-CCSD	2.95
	EOM-SF(2,3)	0.96
	EOM-SF(2,3)	0.32
	MR-CISD(2,2)	0.57
	MR-CISD+Q(2,2)	0.16
48	CCSD(T)	10.58
	CCSD(Δ)	3.42
	CCSD(T) <sub>Δ</sub>	2.72
	CCSD(Δ) <sub>T</sub>	1.80
	OD(T)	6.03
	OD(Δ)	4.69

not change sign like that of CASPT2 and MRCISD(TQ) [MRCISD with perturbative inclusion of triple and quadruple excitations] level calculations.<sup>45</sup> We note that the EOM-SF-CCSD [spin-flip (SF) equation-of-motion (EOM) CC],<sup>46</sup> CCSD(T)<sub>Δ</sub> [asymmetric perturbative triples corrected CCSD],<sup>48</sup> and OD(T) [symmetric perturbative triples corrected OD]<sup>48</sup> error surfaces change sign. IVO-SSMRPT(2,2)/6-31G\* yields tolerable deviations from the FCI values exhibiting a maximum and a minimum error of the order of 7.82 and 1.22 kcal mol<sup>-1</sup>, respectively. In fact, the SSMRPT method with CASSCF(2,2) and IVO-CASCI(2,2) yields NPEs of 6.4 and 6.6 kcal mol<sup>-1</sup>, respectively and therefore, the orbitals as well as CI-coefficient optimization in the zero-order level do not noticeably improve the performance of the

SSMRPT method. Note that the SSMRPT level of calculation suffers from the noticeable NPE, indicating that coupling among amplitudes within  $T^4$  can be important. In ref. 45, we found that the absolute maximum and minimum errors against the FCI for the CASPT2(2,2) method are 13.41 and 12.24 kcal mol<sup>-1</sup> respectively, which are considerably larger than that of our IVO-SSMRPT and CASSCF-SSMRPT with CAS(2,2) estimates. The corresponding errors for CASPT2(4,4) are 7.62 and 6.06 kcal mol<sup>-1</sup>. The NPEs for the CASPT2(2,2) and CASPT2(4,4) methods are 1.17 and 1.56 kcal mol<sup>-1</sup>, respectively.<sup>45</sup> The CASPT2(8,8)/6-31G\* and MRCISD[TQ](8,8)/6-31G\* calculations lead to smaller NPEs which are 1.56 and 1.33 kcal mol<sup>-1</sup>, respectively.<sup>45</sup> In Fig. 2, we see that the error is higher at very small C–H bond distances. In the intermediate region, where the nature of the wave function of the C–H bond experiences fast changes, SSMRPT with both CASSCF and IVO-CASCI orbitals are the most parallel to FCI within 1 kcal mol<sup>-1</sup> while EOM-SF(2,3), and its less expensive active-space counterpart EOM-SF(2,3) are within 0.2 kcal mol<sup>-1</sup> of FCI. In this region, the NPE of the free-valence CASPT2 is also very small, being 0.1 kcal mol<sup>-1</sup>. It should be mentioned that the methods which faithfully reproduce the character change of the wave function in the intermediate region can yield small NPEs in this region.

Fig. 3 and 4 correspond to the total energy and error surfaces, respectively, for C–H bond dissociation for the second geometry where the C–H bond length was varied from 1.05 to 4.23 Å.<sup>46</sup> In the case of the second geometry, we gauge our results of the IVO-SSMRPT method against the MRCISD+Q(2,2) results of Krylov and coworkers<sup>46</sup> along the dissociation surface that leads to planar CH<sub>3</sub>. The IVO-SSMRPT/aug-cc-pVTZ surface faithfully parallels to MRCISD(2,2)+Q as the errors provided by the method are acceptably small over the entire C–H distances (including equilibrium and elongated regions) treated here (maximum and minimum errors are 4.65 and 2.81 kcal mol<sup>-1</sup>, respectively) and yields an NPE of 1.84 kcal mol<sup>-1</sup>. The CASSCF-SSMRPT method also provides a similar dissociation error surface (maximum and minimum errors are 5.68 and 4.08 kcal mol<sup>-1</sup>, respectively) to that of the IVO-SSMRPT one, the corresponding

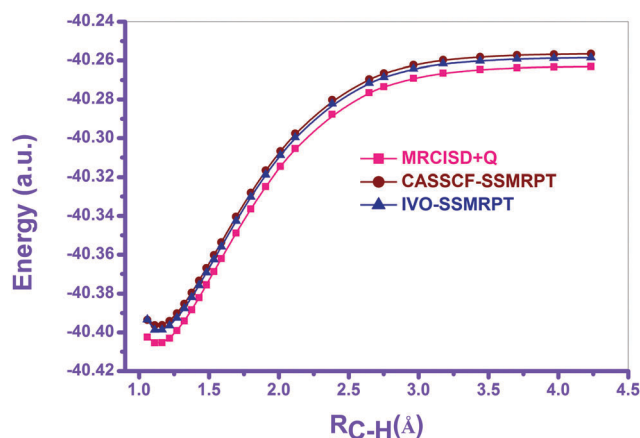


Fig. 3 Plot of the IVO-SSMRPT energies along with MR-CISD+Q results along the C–H bond breaking coordinate in methane with the aug-cc-pVTZ basis set.

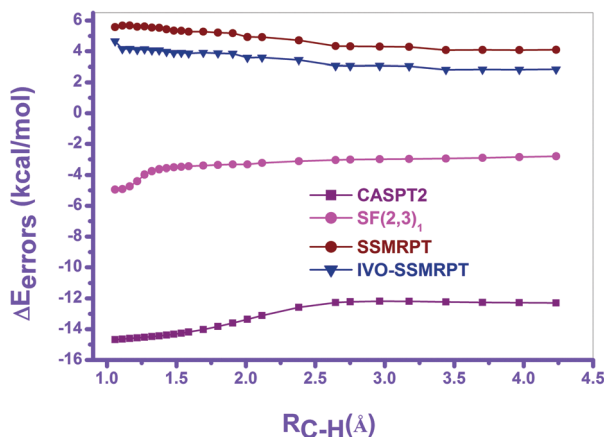


Fig. 4 Error surfaces of IVO-SSMRPT(2,2) and other selected methods against MRCI+Q results (Krylov and coworkers<sup>46</sup>) in the aug-cc-pVTZ basis as a function of the length of a single C–H bond for methane with the CH<sub>3</sub> radical frozen in a planar geometry.

NPE being 1.60 kcal mol<sup>-1</sup>. Note that similar to the small basis 6-31G, there is also no change of sign of the deviation for both IVO-SSMRPT and CASSCF-SSMRPT. The CASPT2 and EOM-SF(2,3) levels of computation provide very similar results to that of our estimates, yielding NPEs of 2.5 and 2.14 kcal mol<sup>-1</sup>, respectively.<sup>46</sup> The EOM-SF-CCSD and EOM-SF(2,3) methods provide almost identical estimates and yield NPEs of 0.99 and 0.51 kcal mol<sup>-1</sup>, respectively.<sup>46</sup> At this point, we want to stress that the GVVPT2/cc-pVTZ level of calculation with CASSCF(8,9) provides a NPE of 5.1 kcal mol<sup>-1</sup>.<sup>47</sup> Although CCSDT-2, CCSDT-1a and CCSDT-1b surfaces exhibited NPEs around 4.5 kcal mol<sup>-1</sup>, the CCSD+T(CCSD) composite scheme yields a larger NPE of 9.9 kcal mol<sup>-1</sup>.<sup>47</sup> Not surprisingly, the MBPT provides larger NPEs (kcal mol<sup>-1</sup>): 12.4 for D-MBPT(4), 8.0 for SD-MBPT(4), 11.1 for SDT-MBPT(4) and 7.3 for SDTQMBPT(4).<sup>52</sup>

We now focus on the dissociation energy of C–H. At each C–H bond length, the angle and the C–H bond distances in the CH<sub>3</sub><sup>\*</sup> have been optimized using the IVO-SSMRPT numerical gradient approach. The predicted C–H dissociation energy,  $D_e$  (kcal mol<sup>-1</sup>) of 116.7 at the IVO-SSMRPT(2,2)/aug-cc-pVTZ level is in close agreement with that found at previous high levels of calculations,<sup>47,52</sup> e.g. 109.8 at GVVPT2(8,9)/cc-pVTZ, 109.5 at the MRD-CI/6-31G\* extrapolated to FCI level and 109.2 at the CCSDT-1a/DZP level, and is close to the experimental value of 112.4. The dissociation energy calculated at the MRCISD/6-311++G(df,p) level is somewhat low (104.3 kcal mol<sup>-1</sup>)<sup>44</sup> compared with the experimental finding.

Like the CASPT2 and EOM-SF-based methods, our IVO-SSMRPT method may also provide adequate results for kinetics modeling of reactions involving a CH<sub>4</sub> molecule. Keeping in mind the second-order perturbative nature of the theory, the performance of the IVO-SSMRPT(2,2) method seems to predict the CH<sub>4</sub> dissociation potential in close agreement with the computationally demanding higher-order CC and MRCI approaches.

**2. C–C bond breaking in the ground state ethane: C<sub>2</sub>H<sub>6</sub> → 2CH<sub>3</sub>.** We next tested the performance of the IVO-SSMRPT method for the C–C bond dissociation of the ground state ethane

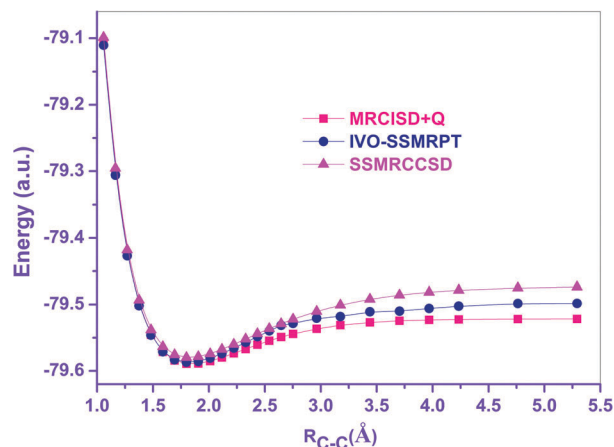


Fig. 5 Potential energy surfaces along the C–C bond stretching for ethane in the aug-cc-pVTZ basis set.

as there are various established results available.<sup>46,53–55</sup> The ground state of ethane may be more appropriately described by the two-configuration wave function:  $(\text{core})^4(\sigma_g)^2(\sigma_u^*)^2(\sigma_u)^4 - \gamma(\text{core})^4(\sigma_g)^2(\sigma_u^*)^2(\sigma_u)^4(\sigma_g^*)^4(\sigma_g)^0(\sigma_u^*)^2$  where the coefficient  $\gamma$  depends on the C–C bond distance and it is small near the equilibrium region and increases with the elongation of the bond-length, as the wave function acquires MR nature. Therefore, the said C–C bond distance is known to require a minimum CAS(2,2) reference space for its correct description. The present calculation is performed in the aug-cc-pVTZ basis set, keeping the two core as well as two virtual orbitals frozen.

Fig. 5 describes the IVO-SSMRPT dissociation energy surface corresponding to the C–C bond in ethane due to the variation of the C–C bond from 1.05 to 5.29 Å, with the methyl groups frozen at planar staggered configuration and  $R_{C-H} = 1.084819$  Å as in ref. 46. We have also assembled the PES provided by the MR-CISD+Q level of calculation.<sup>46</sup> The error surfaces with respect to the MR-CISD+Q estimate appear in Fig. 6. As the SSMRPT and IVO-SSMRPT methods give very close results, here we report only the latter. The IVO-SSMRPT calculations provide

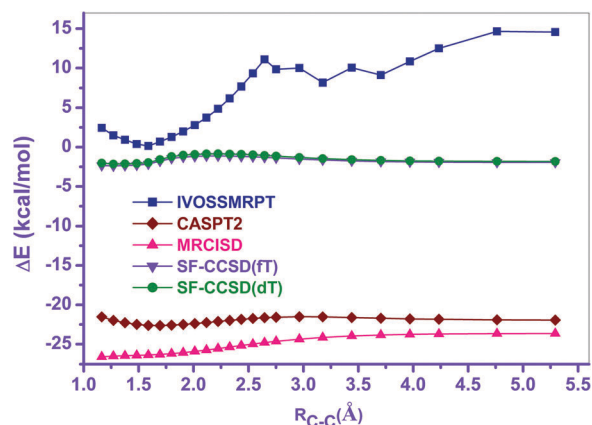


Fig. 6 Error energy surfaces with respect to the MR-CISD+Q estimates<sup>46</sup> as a function of the C–C bond dissociation for ethane in the aug-cc-pVTZ basis set.

a smooth and consistent behavior across the entire PES between the equilibrium and the dissociation limit. Note that the IVO-SSMRPT parallels the MRCISD+Q surface very well and stays close to the MR-CISD+Q.<sup>46</sup> As shown in Fig. 5, the IVO-SSMRPT method underestimates the bond dissociation energy as it yields relatively low energies at large C–C bond lengths. With respect to the MRCISD+Q values, the IVO-SSMRPT method yields the maximum and minimum absolute errors of 14.65 and 0.13 kcal mol<sup>-1</sup>, respectively providing an NPE of around 14.5 kcal mol<sup>-1</sup>. The CASPT2 and MR-CISD methods also provide accurate PESs with the NPEs of 1.8 (with the maximum and minimum absolute errors of 22.63 and 20.83 kcal mol<sup>-1</sup>, respectively) and 3.10 (with the maximum and minimum absolute errors of 26.74 and 23.63 kcal mol<sup>-1</sup>, respectively) kcal mol<sup>-1</sup>, respectively. Golubeva *et al.*<sup>46</sup> demonstrated that the size-extensive (Davidson) correction accounts for around 3 kcal mol<sup>-1</sup> of the NPEs. We have already mentioned that the IVO-SSMRPT method is size-extensive, while CASPT2 suffers from not being size-extensive. Here, it is worth noting that the NPEs along the entire dissociation surface are 1.13, 1.27, and 1.29 kcal mol<sup>-1</sup> for SF-CCSD, SF-CCSD(dT), and SF-CCSD(fT), respectively [where dT and fT stands for diagonal and Fock triples, respectively].<sup>53</sup> We now iterate the important observations made by Yang *et al.*<sup>55</sup> for ethane using various CC and MR-based methods with the cc-pVDZ basis. The RCCSD(T) [restricted CCSD(T)] energy surface of C–C bond dissociation in C<sub>2</sub>H<sub>6</sub> has an unphysical hump around 2.2 Å, as observed earlier by Yang *et al.*<sup>55</sup> which indicates the breakdown of the RCCSD(T) method, suggesting that nonperturbative triple excitations and genuine MR treatments need to be considered. It should be mentioned that the RCR-CCSD(T) [restricted completely renormalized CCSD(T)] approach<sup>3</sup> eliminates the hump in the PES and is able to correctly describe the C–C bond dissociation in ethane, however, the errors increase with the bond length.<sup>55</sup> As shown in ref. 55, CASPT2, CASPT3 [third-order CASPT], MRCISD, MR-ACPF [multireference averaged coupled-pair functional], and MR-AQCC [multireference averaged quadratic CC] are also very useful to recover correlation energy, with the largest discrepancy of 4 kcal mol<sup>-1</sup> relative to RCCSDT(2)<sub>Q</sub> (CC singles, doubles and triples augmented with second-order perturbative quadruples corrections)<sup>56</sup> for ethane. The overall errors yielded by the IVO-SSMRPT method are comparable with the error bars of the computationally demanding estimates.

**3. O–O bond-breaking in H<sub>2</sub>O<sub>2</sub> (→2OH).** The O–O bond breaking in H<sub>2</sub>O<sub>2</sub> is a paradigmatic case where the dynamical electron correlation effect brings a vital contribution to the bonding. It is known that the nondynamical correlation in the O–O at the equilibrium region is not significant. Akin to the situation in F<sub>2</sub>, the RHF solution is unbound just a small O–O bond length away from the equilibrium distance.

Here, we have employed the same basis and scheme as those used in recent benchmark studies of Yang *et al.*<sup>55</sup> for the cc-pVDZ basis set. During the change of O–O bond length, other equilibrium geometrical parameters of H<sub>2</sub>O<sub>2</sub> [taken from experiment<sup>57</sup>] are kept frozen. In our calculations, excitations of the 1s electrons of O are excluded. The energies obtained by the

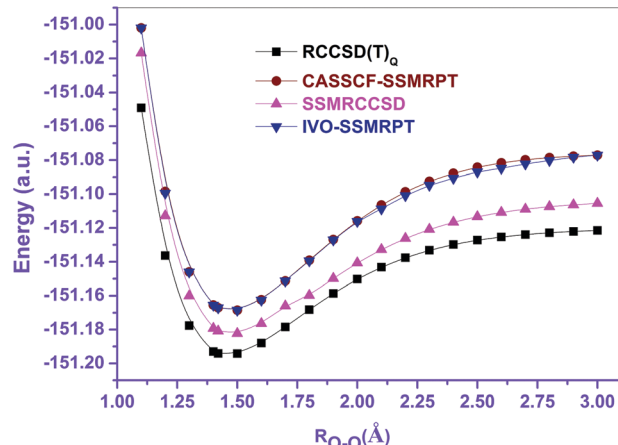


Fig. 7 Dissociation energy surfaces of the O–O bond in H<sub>2</sub>O<sub>2</sub> generated via the IVO-SSMRPT and RCCSDT(2)<sub>Q</sub><sup>55</sup> methods for the cc-pVDZ basis set.

IVO-SSMRPT and CASSCF-SSMRPT level of calculations using a minimal (2,2) active space are plotted as a function of O–O in Fig. 7 along with the RCCSDT(2)<sub>Q</sub> and SSMRCCSD results. The error surfaces relative to RCCSDT(2)<sub>Q</sub> are described in Fig. 8. The present analysis indicates that SSMRPT can be a useful alternative to RCCSDT and SSMRCCSD when the biradicaloids are too large for CC methods. Both the figures illustrate the effectiveness of IVO-SSMRPT to recover correlation energy over the entire bond distances considered here. The topology of the IVO-SSMRPT and CASSCF-SSMRPT energy surface agrees well with the computationally expensive RCCSDT(2)<sub>Q</sub> and SSMRCCSD results, indicating that with IVO-CASCI as well as CASSCF reference wave functions, the SSMRPT method is able to yield qualitatively correct PESs. The comparison with RCCSDT(2)<sub>Q</sub> results shows that the IVO-SSMRPT level of computation overestimates the dissociation energy as it picks up less electron correlation effects at large O–O bonds than near the equilibrium zone, which is evident from the larger deviations [relative to RCCSDT(2)<sub>Q</sub>] at elongated bond distances than those at equilibrium values.

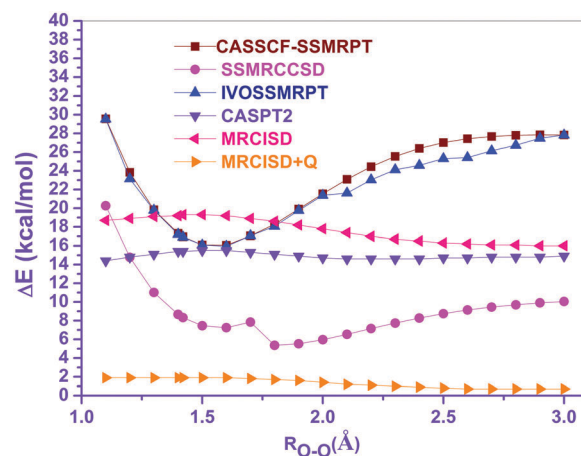


Fig. 8 Errors of IVO-SSMRPT energies relative to RCCSDT(2)<sub>Q</sub><sup>55</sup> of H<sub>2</sub>O<sub>2</sub> at different O–O bond lengths for the cc-pVDZ basis set.

It has been observed from the work of Yang *et al.*<sup>55</sup> that other MR-based methods MR-AQCC, MR-ACPF, MRCISD, MR-CISD+Q, CASPT2, and CASPT3 recover more (over estimate) electron correlation effect at elongated bond distances than near the equilibrium region leading to underestimation of the bond dissociation energies. In this context, we also mention another example that although CASPT3 recovers more correlation energy compared to CASPT2, the performance of the former is not better than the latter as the errors of CASPT3 are more sensitive with altering the bond-distances.<sup>55</sup> Despite the RCCSD(T) level of calculations for H<sub>2</sub>O<sub>2</sub> providing a tiny unphysical hump on the computed PESs at relatively small values of the O–O bond length, RCCSD(T) is useful to recover correlation energy near the equilibrium region.<sup>55</sup> The RCR-CCSD(T) method<sup>3</sup> provides the correct dissociation profile of the O–O in H<sub>2</sub>O<sub>2</sub>; however, it is not very useful to recover electron correlation effects as it produces noticeable errors<sup>55</sup> with respect to RCCSD(T)<sub>Q</sub> with the elongation of the bond-distances and hence provides high dissociation energy. The errors of the IVO-SSMRPT, CASSCF-SSMRPT and SSMRCCSD methods relative to RCCSD(T)<sub>Q</sub> have maxima at the intermediate bond dissociation region, similar to that of UCCSD, UCCSD(T), and UCRCCSD(T) [unrestricted CRCCSD(T)]. The error surfaces denote that SSMRPT with both CASSCF and IVO-CASCI reference wavefunctions is very discernible at recovering correlation energy, with an average deviation relative to RCCSD(T)<sub>Q</sub> being around 25 kcal mol<sup>-1</sup>. The performance of the CASPT2 method is marginally better than that of MRCISD and SSMRPT methods as the errors of CASPT2 do not change much at different O–O bond distances. MRCISD+Q provides a very accurate dissociation surface with almost constant absolute errors relative to RCCSD(T)<sub>Q</sub> close to 1 kcal mol<sup>-1</sup> at different bond lengths. Another way to judge the quality of the method used to compute energy surface is to compare bond dissociation energies with the experimentally estimated data. IVO-SSMRPT predicts the dissociation energy for the O–O bond in H<sub>2</sub>O<sub>2</sub> of 51.13 kcal mol<sup>-1</sup> which is in good agreement with MRCI-SD/cc-pVTZ and CASPT2/ANO values of 52.72 and 51.57 kcal mol<sup>-1</sup>,<sup>58</sup> respectively and these agree with the experimental data of 54.45 kcal mol<sup>-1</sup>. Therefore, the potential energy well depths are considerably underestimated by all these theoretical methods with respect to the experiment, by around 2–3 kcal mol<sup>-1</sup>.

## B. Double-bond breaking

The computation of the double-bond dissociation surface is a typical example symbolizing the limitations of various conventional *ab initio* methods. For the multiple-bond dissociation process, the correlation (interaction) between the different bonds may have a crucial effect in the proper description and dissociation of multiple bonds.

**1. C=C bond breaking of ethylene: C<sub>2</sub>H<sub>4</sub> ⇌ 2CH<sub>2</sub>.** We now consider the dissociation of the CC double bond breaking in ethylene (singlet) to form two methylenes (triplet) for the ground state. C<sub>2</sub>H<sub>4</sub> ⇌ 2CH<sub>2</sub> is the simplest example for the direct breakage of a double bond. Such a dissociation involves the rupture of both  $\sigma$  and  $\pi$  bonds, obviating the need to

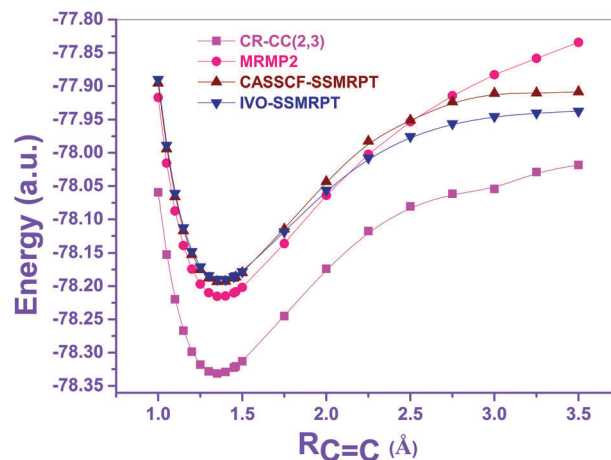


Fig. 9 Potential energy surfaces along the C=C bond breaking coordinates of ethylene (frozen core).

consider the interaction among ( $\sigma, \sigma^*$ ) and ( $\pi, \pi^*$ ) orbitals. As the dissociation geometry is approached, ( $\sigma, \sigma^*$ ) and ( $\pi, \pi^*$ ) orbitals become degenerate. A balanced description of such a dissociation profile needs a truly MR description and has been studied in detail.<sup>59,60</sup> In the ground state, where orbital symmetry is conserved, the  $\pi$ -bond breaks before the  $\sigma$ -bond. The present calculation is carried out with the Huzinaga-Dunning polarized double- $\zeta$  (DZP) basis set and keeping all other degrees of freedom frozen at  $R_{\text{CH}} = 1.079 \text{ \AA}$ , and  $\angle \text{HCH} = 120^\circ$ .<sup>61</sup> This system has been treated using a CAS with four electrons in four active orbitals. SSMRPT dissociation PESs of the C=C bond of ethylene are summarized in Fig. 9, which we compare with MRMP2<sup>9</sup> and CR-CC(2,3) [CR-CC with singles, doubles, and non-iterative triples]<sup>3</sup> results. Table 2 shows the calculated dissociation energy of C=C bond-breaking in ethylene. In general, the SSMRPT results are competitive with the estimates of the CC level of computations but at lesser cost. Note that the CR-CC(2,3) surface exhibits an unphysical shape in the dissociation region suggesting that higher-order excitations are important for a quantitatively correct description of the dissociation region. All MRPT surfaces are smooth and exhibit qualitatively correct behavior up to the dissociation limit. Like that of other test cases, the dissociation profiles of the IVO-SSMRPT method have close resemblance with the CASSCF-SSMRPT one even for the multiply bonded molecule. Although the behavior of the SSMRPT and MRMP2 surfaces is very similar up to intermediate distances, the main discrepancies are observed at the dissociation limit where MRMP2 energies increase too fast with C=C coordinates and the corresponding dissociation energy is overestimated compared to the SSMRPT level of calculation.

Table 2 Dissociation energy (kcal mol<sup>-1</sup>) for C=C bond breaking in ethylene in DZP basis set

Method	Dissociation energy
IVO-SSMRPT	180.02
CASSCF-SSMRPT	184.14
MRMP2	204.87



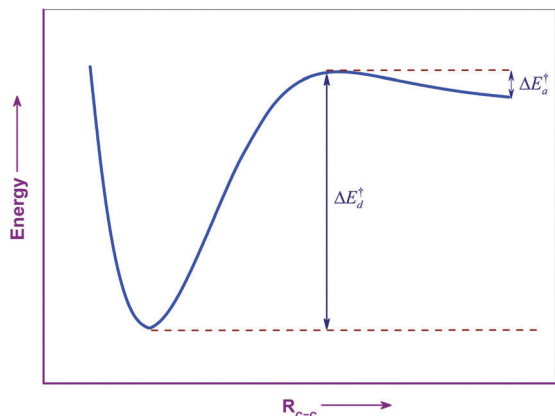


Fig. 10 The dissociation energy surface of  $T_1$  ketene along the reaction coordinate. The reaction coordinate corresponds to the distance between the carbon atoms. Here  $\Delta E_d^\ddagger$  and  $\Delta E_a^\ddagger$  characterize the (classical) dissociation and association barriers, respectively.

This observation also suggests that MRMP2 recovers less correlation energy than IVO-SSMRPT. Fig. 9 clearly indicates the ability of the SSMRPT method to capture the diradicaloid character of the wave function along the C=C bond breaking coordinates.

## 2. Fragmentation of triplet ketene via C=C bond fission.

We now focus on the bond dissociation potential profile for the photodissociation of  $T_1$  ketene:  $H_2 CCO \rightarrow CH_2 (\tilde{X}^3B_1) + CO$ , illustrated in Fig. 10. The photofragmentation of ketene has long been a subject of numerous experimental<sup>62</sup> and theoretical<sup>63–69</sup> studies which can be used as a database to examine the performance of our method. The ketene molecule in the ground singlet state ( $S_0$ ) is first excited to the  $S_1$  excited state, the excited ketene undergoes nonadiabatic transition to  $S_0$  or  $T_1$  (triplet state), and finally dissociates to  $CH_2$  and  $CO$  with the C=C bond fission on either  $S_0$  or  $T_1$  (see Fig. 10). The experimentally observed photodissociation process indicates that the dissociation rate of triplet ketene,  $k(E)$ , exhibits a steplike structure as a

function of total energy near the dissociation threshold that can be described as emerging from the vibrationally quantized bottleneck states [can be viewed as the eigenstates of an “activated complex” in the traditional transition state theory] at the transition state (TS). In order to reproduce the step structure seen experimentally, the imaginary frequency ( $\omega^\ddagger$ ) at the transition state of the triplet ketene needs to be approximately  $50\text{--}100\text{ cm}^{-1}$ .<sup>65,69</sup> A literature survey<sup>63–65,68,69</sup> suggests that the origin of the observed step-like structure is not clear. In all the calculations, we have used IVO-CASCI(2,2) as a zero-order function and cc-pVXZ (X = D and T) basis sets employing the same scheme as reported by Ogihara *et al.*<sup>69</sup> [the core orbitals of C and O atoms are kept frozen]. The experimentally estimated barrier on the  $T_1$  surface is about  $3\text{ kcal mol}^{-1}$ <sup>62</sup> suggesting that a well-defined barrier height exists that may rule out any possible steps *via* a tunneling mechanism. Note that a steplike structure in  $k(E)$  has also been found in the case of singlet ketene photochemical decomposition where the energy surface increases monotonically without facing any barrier for the reverse association reaction and thus no tunneling occurs for the forward photodissociation process and hence the noticed steps in  $k(E)$ .

We have assembled in Fig. 11, the dissociation of triplet ketene (into methylene and carbon monoxide) obtained at the IVO-CASCI, and IVO-SSMRPT levels with cc-pVXZ (X = D and T) basis sets. For comparison, we also plot the results of the IVO-CASCI based SSMRCCSD method [that has the ability to yield highly accurate energies] in the same figure. The discontinuities are not visible on the computed PESs by IVO-SSMRPT and other MR-based methods.<sup>69</sup> Fig. 11 suggests that the photoreactions of triplet ketene passes through a well characterized tight TS. Keeping in mind the figures of Yamamoto and coworkers<sup>69</sup> along with the present work, one can find that the local topological shape of the computed potential barrier is rather identical among different levels of computation, although the difference of shape provided by various methods is prominent

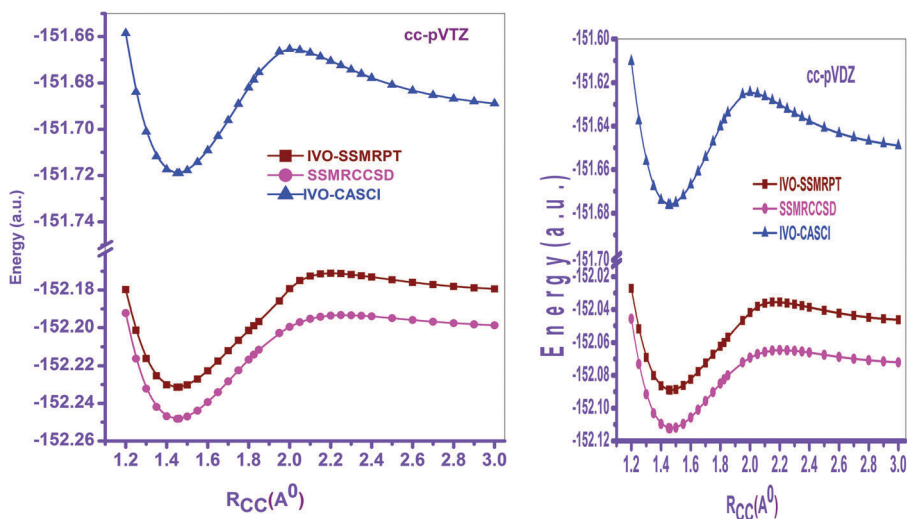


Fig. 11 Potential energy surfaces of photodissociation pathways of triplet ketene [ $\rightarrow^3CH_2 + CO$ ] obtained at several different levels of electronic structure theory.

in the region of the reactant and the product. A comparison of energy profiles obtained at the IVO-CASCI and other higher-order methods indicates that the results of the former method differ significantly from the latter, especially in the portion of TS. This is because IVO-CASCI cannot handle the dynamic electron correlation and thus, for this region, one should carefully consider the MR methods. Similar findings are also observed in the case of CASSCF and MRMP2 calculations.<sup>69</sup> Fig. 11 indicates that although IVO-CASCI has the correct shape, it is slightly higher in energy as IVO-CASCI does not incorporate the dynamic correlation effect, while the IVO-SSMRPT method is very close to the SS-MRCCSD method. Note the good and consistent close similarity between the PESs provided by IVO-SSMRPT and the expensive MRCC calculations by Ogihara *et al.* [see figures reported in ref. 69]. Therefore, IVO-SSMRPT has sufficient flexibility to model the large changes of the electronic structure in the dissociation reaction of T<sub>1</sub> ketene. To judge the quality of our results, the barrier heights extracted from the computed association–dissociation surfaces [see Fig. 10 for definition] are summarized in Table 3. It is difficult to present a unified quantitative comparison between the approaches assembled in the table because of the use of different basis sets and sizes of the CAS.

The large values for both association and dissociation processes guarantee a substantial barrier on the PES of triplet ketene. The figure and table indicate that the potential surface needs to dwindle from the TS towards the product zone asymptotically by 3 kcal mol<sup>-1</sup> in order to reach the experimental estimate. The association barrier is significantly overestimated by the IVO-CASCI(2,2) and CASSCF(14,11) levels of calculation since the experimentally observed association barrier (includes zero-point energy and tunneling effects) is 3.66 ± 0.05 kcal mol<sup>-1</sup>.<sup>69</sup> Like in earlier works,<sup>69</sup> we observed that the incorporation of the dynamic correlation to IVO-CASCI using the SSMRPT method decreases this overestimation significantly, although

it has been seen that the MR-correlated methods always (marginally) overestimate the association barrier against the experimental estimate. As shown in Table 3, the dissociation (association) barrier height rises (abbreviates) with an enlarging basis set size indicating that the anharmonicity of the potential profile enhances with the size of the basis sets used in the calculations. The present IVO-SSMRPT/cc-pVTZ calculations reveal that a barrier height of 4.68 kcal mol<sup>-1</sup> is required for the association of triplet ketene. It should be pointed out that the association barrier amounts to 6.01 kcal mol<sup>-1</sup> at the IVO-SSMRPT/cc-pVDZ level of theory which would be corrected toward database value by using the cc-pVTZ basis. Allen and Schaefer<sup>64</sup> found the transition state to be 4.74 kcal mol<sup>-1</sup> above the products at the CCSD/TZ(2df,2p) level. Note that the Mk-MRCCSD association barrier for the process without zero-point energy correction is 6.50 kcal mol<sup>-1</sup> with the cc-pVDZ basis, whereas it is 5.03 kcal mol<sup>-1</sup> when an extended basis set, say, cc-pVTZ is employed.<sup>69</sup> The data assembled in the table illustrates that with an increasing level of sophistication of the method, the association barrier is shifted gradually towards the experimental value as the computed estimates of  $\Delta E_a^\ddagger$  become increasingly small. The association barriers provided by the IVO-SMSRPT(2,2) and MRMP2(14,11) methods with the cc-pVTZ basis are consistent with the experimentally measured barrier with a deviation of around 1.0 and 0.3 kcal mol<sup>-1</sup>, respectively. The corresponding value in the case of SS-MRCCSD is 0.16 kcal mol<sup>-1</sup>. Here, it is worth stressing that as seen from the work of Yamamoto and coworkers,<sup>69</sup> the effect of enlarging the CAS is not significant.

In the IVO-SSMRPT calculations, the dissociation barrier is increased from 29.07 kcal mol<sup>-1</sup> with cc-pVDZ to 30.24 kcal mol<sup>-1</sup> with the cc-pVTZ basis. This trend is analogous to that observed for the other MR-based calculations due to Yamamoto and coworkers.<sup>69</sup> At the IVO-SSMRPT(2,2) and MRMP2(14,11) levels

**Table 3** Estimation of dissociation ( $\Delta E_d^\ddagger$ ) and association ( $\Delta E_a^\ddagger$ ) barrier heights (kcal mol<sup>-1</sup>) and imaginary frequency (cm<sup>-1</sup>) at the transition state of triplet ketene by various levels of theory. The experimental estimate includes zero-point energy and tunneling effects

Ref.	Method	$\Delta E_d^\ddagger$	$\Delta E_a^\ddagger$
Present	IVO-CASCI(2,2)/cc-pVDZ	38.11	19.04
	IVO-CASCI(2,2)/cc-pVTZ	36.02	14.88
	IVO-SSMRPT(2,2)/cc-pVDZ	29.07	6.01
	IVO-SSMRPT(2,2)/cc-pVTZ	30.24	4.68
69	Mk-MRCCSD(2,2)/cc-pVDZ	24.53	6.50
	Mk-MRCCSD(2,2)/cc-pVTZ	27.49	5.03
	Mk-MRCCSD(2,2)/cc-pVQZ	28.51	4.70
	CCSD/cc-pVDZ	24.11	6.11
	CCSD/cc-pVTZ	27.11	4.74
	CCSD/cc-pVQZ	28.09	4.42
64	CCSD/TZ(2d1f,2p)	27.91	4.74
	UCCSD(T)/cc-pVQZ/TZ (+correlation correction)	29.77	2.99
69	CASSCF(14,11)/cc-pVTZ	16.34	14.49
	MRMP2(14,11)/cc-pVTZ	29.33	3.39
	Ad-MRCCSD (4 × 4 CAS)/cc-pVDZ	23.59	5.56
	Ad-MRCCSD (8 × 4 CAS)/cc-pVDZ	22.99	5.68
	Ad-MRCCSD (4 × 8 CAS)/cc-pVDZ	23.85	4.78
	MRACPF (14,11)/cc-pVTZ	28.35	4.74
62	Experiment		3.66 ± 0.05

with the cc-pVTZ basis, the  $T_1$  dissociation barrier is found to be 30.24 and 29.33 kcal mol<sup>-1</sup>, respectively which is in close agreement with the UCCSD(T) result (29.77 kcal mol<sup>-1</sup>). Although the agreement between the two MR-based mean field values is very satisfactory, it should be noted that the  $T_1$  dissociation energy profile at the CASSCF/IVO-CASCI level is qualitatively poor, IVO-CASCI (and CASSCF) yielding a significantly overestimated (and underestimated) dissociation height compared to other sophisticated estimations. The present analysis underlines the significance of the incorporation of dynamical correlation in the computation of energy surfaces

of triplet ketene. Table 3 shows that the barriers at the Mk-MRCCSD(2,2) level are very close to that at the IVO-SSMRPT(2,2) level.

Table 4 shows that our estimates are in pleasing agreement with much more extensive MRMP2 calculations of Yamamoto and coworkers.<sup>69</sup> The MRMP2(14,11)/cc-pVTZ level of calculation identified the TS for the ketene triplet dissociation at 2.312 Å whereas our IVO-SSMRPT(2,2)/cc-pVTZ method gave a value of 2.1484 Å. The corresponding value provided by the UCCSD(T)/cc-pVQZ/TZ/(+correlation correction) scheme is 2.257 Å. Note that at the TS, the C–C bond is extended by about 48% (0.7 Å) relative to the ground state. Fig. 11 also indicates that with the incorporation of dynamical correlation, the IVO-CASCI TS location is shifted gradually toward the product region. Here, we recall the previous investigations by Yamamoto and coworkers using the CASSCF and MRMP2 methods.<sup>69</sup> The calculated vibrational frequencies [which often serve as a critical test for the accuracy of the methods] for the reactants, and transition states on  $T_1$  surface using the IVO-based gradient scheme are summarized in Table 5. These results show that the IVO-SSMRPT calculation also delivers consistent results for the vibrational frequencies. We should notice at this point that the IVO-SSMRPT, using the minimal active space consisting of two electrons in the two orbitals, correctly accounts for the trend of the vibrational frequencies provided by the CASSCF(14,11)-MRMP2 protocol. It can be seen from Table 5 that MRMP2 predicts a much lower CO stretching frequency for the reactant (1679 cm<sup>-1</sup>) than the IVO-SSMRPT estimate, while CCSD predicts a frequency of 1859 cm<sup>-1</sup>, being close to the IVO-SSMRPT and SSMRCCSD values (1841.68 and 1839.22 cm<sup>-1</sup>, respectively). The reason for such a noticeable disagreement between IVO-SSMRPT and MRMP2 is not clear to us as the experimental data are not known for this system. However, the discord is unexpected as per

**Table 4** Optimized geometrical parameters [bond lengths (Å), and bond angles (°)] of the reactant, transition state, and product for the triplet ketene surface for the cc-pVTZ basis. The entries in parentheses indicate the corresponding values using the cc-pVDZ basis

State	Parameter	IVO-SSMRPT	SSMRCCSD	MRMP2 <sup>69</sup>
Reactant	C–C	1.4493(1.4665)	1.4501(1.4682)	1.461
	C–H <sub>1</sub>	1.0826(1.0973)	1.0838(1.0994)	1.083
	C–H <sub>2</sub>	1.0753(1.0904)	1.0774(1.0935)	1.077
	C–O	1.1945(1.2023)	1.1895(1.1982)	1.203
	∠ H <sub>1</sub> CH <sub>2</sub>	120.124(119.956)	120.227(120.033)	120.1
	∠ H <sub>1</sub> CC	120.075(120.277)	119.803(120.020)	120.0
	∠ CCO	127.175(126.574)	127.936(127.325)	126.2
	C–H	1.0728(1.0895)	1.0772(1.0947)	1.077
Product	C–O	1.1383(1.1464)	1.1286(1.1383)	1.141
	∠ HCH	133.126(131.785)	133.326(132.169)	134.0
	C–C	2.1484		2.312
	C–H <sub>1</sub>	1.0770		1.079
	C–H <sub>2</sub>	1.0743		1.077
TS	C–O	1.1457		1.148
	∠ H <sub>1</sub> CH <sub>2</sub>	130.513		132.3
	∠ H <sub>1</sub> CC	115.219		113.6
	∠ CCO	113.987		113.8

**Table 5** Vibrational frequencies (cm<sup>-1</sup>) for the reactant, transition state, and product geometries for the triplet ketene surface for the cc-pVTZ basis. The entries in parentheses indicate the corresponding values using the cc-pVDZ basis

State	Mode	IVO-SSMRPT	SSMRCCSD	MRMP2 <sup>69</sup>	CCSD <sup>64</sup>
Reactant	CC-Stretching	983.89(973.24)	983.23(969.58)	911	988
	Asym-CH-stretching	3332.75(3340.43)	3258.93(3294.85)	3355	3279
	Sym-CH-stretching	3175.08(3179.42)	3134.46(3148.65)	3188	3139
	CO-Stretching	1841.68(1842.65)	1839.22(1842.98)	1679	1859
	CH <sub>2</sub> -Scissoring	1465.58(1447.83)	1480.80(1442.89)	1418	1460
	CH <sub>2</sub> -Rocking	1056.94(1043.27)	1080.21(1052.43)	1019	1079
	CH <sub>2</sub> -Wagging	804.57(766.19)	821.81(744.37)	727	761
	CCO-Bending	457.96(450.46)	486.48(464.98)	455	474
	Torsion	358.56(349.98)	334.95(388.84)	337	389
	Asymm-CH-stretching	3446.01(3443.85)	3378.83(3375.30)	3431	3374
Product	Symm-CH-stretching	3209.56(3207.40)	3154.40(3151.18)	3162	3152
	CO-Stretching	2112.93(2125.34)	2225.91(2239.16)	2157	2238
	CH <sub>2</sub> -Scissoring	1128.38(1159.44)	1115.48(1131.58)	1071	1110
	Asymm-CH-stretching	3410.60		3431	3344
	Symm-CH-stretching	3180.90		3162	3135
TS	CO-Stretching	2047.85		2060	2141
	CH <sub>2</sub> -Scissoring	1170.51		1123	1167
	CH <sub>2</sub> -Rocking	427.09		344	421
	CH <sub>2</sub> -Wagging	398.74		308	338
	CCO-Bending	224.19		184	228
	Torsion	134.81		108	132

**Table 6** Estimation of the normal mode frequency for CC-stretching at the transition state of triplet ketene ( $\text{cm}^{-1}$ )

Ref.	Method	$\omega^\ddagger$
Present	IVO-SSMRPT(2,2)/cc-pVTZ	386i
64	CCSD/(2df,2p)	379i
	CCSD(T)/(2df,2p)	321i
	UCCSD(T)/cc-pVQZ/TZ	321i
69	MRMP2(14,11)/cc-pVTZ	328i
	MRAQCC(14,11)/cc-pVTZ	344i
	Mk-MRCCSD(2,2)/cc-pVDZ	332i
	Mk-MRCCSD(2,2)/cc-pVTZ	307i
	Mk-MRCCSD(2,2)/cc-pVQZ	310i
	Ad-MRCCSD(4,4)/cc-pVDZ	306i
	Ad-MRCCSD(8,4)/cc-pVDZ	304i

the close resemblance of the formulations. The computational resources needed for SSMRPT are almost similar to those required for the MRMP2 approach. Since the performance of the IVO-SSMRPT method is similar to that of the CC based on SR and MR-descriptions, we hope that the prediction provided by the IVO-SSMRPT method is reliable in this context.

Furthermore, we compare in Table 6 the imaginary barrier frequency,  $\omega^\ddagger$  (corresponding to the C–C<sub>str</sub>) at the transition state estimated with the various levels of methods. The results assembled in Table 6 suggest that values of  $\omega^\ddagger$  depend considerably on the size of the basis set and method used. The barrier frequency at the CCSD and CCSD(T) level of calculation according to King *et al.*<sup>64</sup> is 379i and 321i  $\text{cm}^{-1}$ , respectively. Recently, Yamamoto and coworkers<sup>69</sup> have also carried out an *ab initio* estimation of triplet ketene using the current generation MR-based methods and obtained values of the barrier frequency ranging between 304–344i  $\text{cm}^{-1}$ . IVO-SSMRPT/cc-pVTZ results show that  $\omega^\ddagger$  on the triplet surface is 386i  $\text{cm}^{-1}$  which is slightly higher compared to that under the MRMP2(14,11) estimates (328i  $\text{cm}^{-1}$ )<sup>69</sup> and other dynamically correlated MR-based wavefunction methods.<sup>69</sup> As shown in Table 6, the Mk-MRCCSD and Ad-MRCCSD levels of calculation with cc-pVXZ basis sets provide values of  $\omega^\ddagger$  in the range of 304–332i  $\text{cm}^{-1}$ . It is worth noting that although the value of  $\omega^\ddagger$  changes noticeably with enhancing the basis set size from cc-pVDZ to cc-pVQZ at MR-based level calculations, the effect of increasing the dimension of the active space on  $\omega^\ddagger$  is rather small.<sup>69</sup> One can anticipate from the results of various methods<sup>69</sup> that the  $\omega^\ddagger$  can be reduced by the incorporation of higher-body excitation into the MR-based correlated computations. From the work of Yamamoto and coworkers<sup>69</sup> although one can envision that the value of  $\omega^\ddagger$  can be diminished by increasing the size of the basis sets in conjunction with the size of the reference space, it appears impossible that such a reduction of  $\omega^\ddagger$  becomes as low as 100i  $\text{cm}^{-1}$  even at the CBS level. The barrier frequencies provided by the present IVO-SSMRPT and other MR methods with different CAS and basis sets are in error by a factor of around 3–4 against 100i  $\text{cm}^{-1}$  (maximum value of the imaginary barrier frequency to recover the observed stepwise structure).<sup>65,68,69</sup> Therefore, the barrier frequencies provided by various extensive investigations at the current generation computational models are too large to reveal

any possible steps in  $k(E)$ . This analysis indicates that the correct potential surface in the transition state zone should be much flatter (which governs the extent of tunneling) than the computed surfaces by the methods mentioned here in order to take into account a sufficient shielding of tunneling effects along the reaction coordinate. Consequently, it would be highly desirable to exploit MRCC with a full-blown single-double-triples truncation scheme along with CBS correction in order to meet the experimental observation of the dissociation profile and TS properties. Apart from the error associated with the calculated *ab initio* PESs and hence barrier frequency, Gezelter *et al.*<sup>65</sup> also argued the existence of some other transition states on the triplet PES in the product channel, or nonadiabatic dynamics involving surface-hopping between the triplet and ground state PESs to explain this discrepancy.

Overall, our findings support the conclusion of Yamamoto and coworkers.<sup>69</sup> Restriction of the reference space to two configurations in IVO-SSMRPT calculations does not lead to noticeable errors in the shape of the calculated potential for the triplet state of ketene which further supports the use of IVO-SSMRPT with relatively small CAS in the calculation of the dissociation processes. Similar to that from previous studies,<sup>63–65,68,69</sup> unfortunately, the above discussion clearly reveals that the step-like feature in the observed rate is not reproduced not only at the IVO-SSMRPT and MRMP2 levels but also with MRCC calculations within the assumption that TS vibrational quantization is solely responsible for the steps. Therefore, it looks more fair to accept that some other mechanism is responsible to answer the stepwise rate behavior of the dissociation dynamics of ketene on the triplet surface.<sup>68</sup> At this juncture, we want to mention that a similar discrepancy between theory (300–500  $\text{cm}^{-1}$ ) and experiment (60  $\text{cm}^{-1}$ ) is also noted for the photochemical decomposition of triplet acetaldehyde.<sup>70</sup> Exploring such aspects, however, is beyond the scope of the present work and thus will be discussed in future publications.

### C. Low-lying excited states

To provide a general assessment of the potential of the IVO-SSMRPT method, the low-lying PESs of two species, including the challenging KN diatomic have been considered here.

**1. Bond dissociation of  $\Sigma^+$  and  $\Pi$  states of LiH.** We first illustrate the performance of the IVO-SSMRPT method by computing the PESs for low-lying singlet and triplet states [such as  $X^1\Sigma^+$ ,  $^3\Sigma^+$  and  $^3\Pi$  (lowest stable triplet states)] of the LiH molecule. LiH is one of the smallest diatomic systems, which has been extensively investigated by both theoretical<sup>71–75</sup> and experimental<sup>76</sup> chemists. Although the ground state,  $X^1\Sigma^+$  of LiH is dominated by the single  $1\sigma^22\sigma^2$  electronic configuration around the equilibrium structure, the configurations  $1\sigma^23\sigma^2$  and  $1\sigma^22\sigma^13\sigma^1$  gain in prominence when the Li–H bond is stretched. Therefore, a mixture of these electronic configurations are needed to correctly model the dissociation process of the Li–H bond breaking process. While the excited  $^3\Sigma^+$  state is essentially a singly excited state of the  $2s \rightarrow 3s$  type, the  $^3\Pi$  state is strongly dominated by the single excitation  $2s \rightarrow 3p$ , respectively.

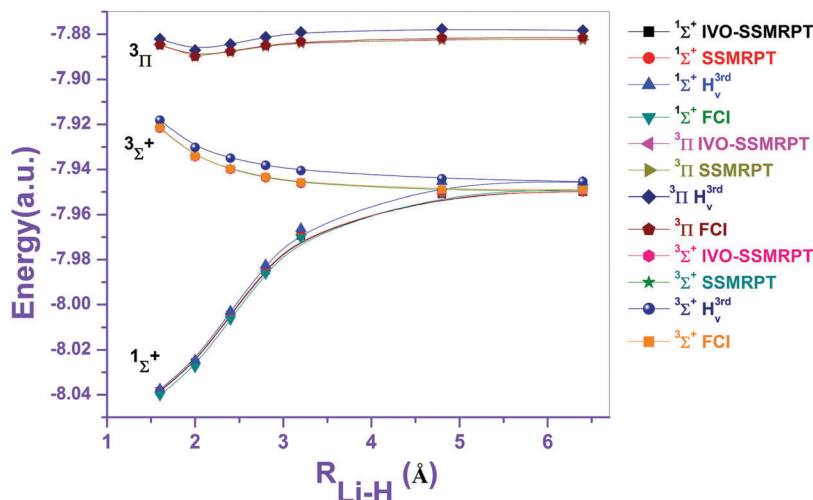


Fig. 12 Plot of the energies of IVO-SSMRPT(2,2) for low-lying electronic states using the cc-pVTZ basis as a function of the internuclear distance for the LiH molecule.

The changing mutual interplay of weak and strong correlation effects along the Li–H bond elongation coordinates makes the molecule a challenging test case for the traditional SR-based *ab initio* methods. Therefore, the dissociation of this four-electron system has always served as a touchstone for quantum chemistry methods tailored to handle quasidegeneracy. Moreover, the role of LiH in the astrophysical and cosmological context is well known and LiH can be considered as a candidate for Stark deceleration owing to its large permanent dipole moment. We use the cc-pVTZ basis set<sup>43</sup> for which the frozen-core FCI<sup>74</sup> results are available over a wide range of geometries. Fig. 12 describes PESs (with increasing internuclear distance up to  $4R_e$ ) for the one lowest singlet- and two triplet-states of LiH obtained by IVO-SSMRPT and CASSCF-SSMRPT methods. Fig. 12 shows that CASSCF-SSMRPT and IVO-SSMRPT are energetically indistinguishable as well as smooth, and both reproduce the same pattern as that of the FCI one. Note that SS-MRPT surfaces with both CASSCF and IVO-CASCI orbitals are in close proximity to FCI. The performance of our SSMRPT method is better compared to the computationally expensive  $H_v^{3rd}$  level of calculation as is evident from the errors of the methods against FCI in terms of their NPE values. We note that NPEs provided by our IVO-SSMRPT (and CASSCF-SSMRPT)  $X^1\Sigma^+$ ,  $^3\Sigma^+$  and  $^3\Pi$  states are 1.30 (1.62), 0.41 (0.36), and 0.49 (0.54) kcal mol<sup>-1</sup>, respectively, whereas the corresponding estimates for the  $H_v^{3rd}$  level of calculation are 1.32, 1.21, and 0.97 kcal mol<sup>-1</sup>, respectively. From the previous works, it has been found that the conventional VU-MRCC and SU-CCSD methods with four-dimensional CAS exhibit divergence in the case of computation of the ground state LiH dissociation because near the equilibrium geometry, the doubly excited  $X^1\Sigma^+$  states extracted by the excited roots of the  $H_{eff}$  would be close in energy to some virtual configurations (providing intruder problems).<sup>71,74</sup> Intruders destroy the reliability of the method. To overcome this problem, one can use a general model space scheme instead of CMS. The figure clearly indicates that dissociation energy surface scanning using the IVO-SSMRPT approach overcomes

the eventual intruder-state problems. It is important to stress that GMS-SUMRCCSD [general model space state-universal CCSD] with the cc-pVTZ basis<sup>74</sup> performs well throughout the entire dissociation coordinates and the NPE values for the  $X^1\Sigma^+$ ,  $^3\Sigma^+$  and  $^3\Pi$  states are 0.158, 0.184 and 0.117 kcal mol<sup>-1</sup>. This fact indicates that the energy surfaces for these low-lying electronic states of LiH yielded at the IVO-SSMRPT (and CASSCF-SSMRPT) level are in good agreement with the computationally more expensive and sophisticated full-blown MRCC (GMS-SUMRCCSD) protocol. Therefore, one can argue that the IVO-SSMRPT approach is intrinsically consistent and capable of providing useful practical results for both ground as well as excited states possessing varying degrees of quasidegeneracy. In addition to the singlet state(s), the IVO-SSMRPT formalism is equally able to treat non-singlet states.

The ground state spectroscopic data [such as the equilibrium interatomic distance ( $R_e$ ), and the harmonic frequency ( $\omega_e$ )] are reported in Table 7 using Dunham's coefficients analysis to the computed PESs. The dissociation energy has been estimated by  $E(3R_e) - E(R_e)$ . The corresponding experimentally known results for this state are also assembled in the same table for comparison. In Table 7, previously published spectroscopic parameters at the CCSD(T) and FCI with aug-cc-pVDZ level are also given for comparison. The accordance of our estimated molecular constants with the available theoretical<sup>73,75</sup> and

Table 7 Selected spectroscopic constants [*viz.* equilibrium bond length  $R_e$  (Å), harmonic vibrational frequency  $\omega_e$  (cm<sup>-1</sup>), and dissociation energy  $D_e$  (kcal mol<sup>-1</sup>)] of LiH

Ref.	Method	$R_e$	$\omega_e$	$D_e$
Present	IVO-SSMRPT	1.601	1423.16	53.09
	CASSCF-SSMRPT	1.608	1421.10	53.31
73	CCSD(T)	1.592	1406.2	56.73
	FCI	1.592	1419.2	58.34
76	Experiment	1.596	1405.65	58.00

experimental database<sup>76</sup> values is encouraging. The key observation is that the relatively small active space is sufficient for the IVO-SSMRPT method and generates the values of the spectroscopic constants provided by the results of the computationally expensive CC method.

**2. KN model molecule: mixing of nonsinglet surfaces.** In our next exploration, we have considered the computation of PESs of some low-lying non-singlet states of experimentally unknown diatomic molecule KN *via* the IVO-SSMRPT method. This fascinating molecule is ionic at equilibrium geometries with high dipole moment but dissociates to a neutral asymptote. Therefore, an important change occurs in the electronic states as the internuclear distance changes. From the spectroscopic point of view, this system is very interesting due to the unusual shapes of the energy surfaces (far from harmonic or Morse behavior) and unusual bonding. Thus, the description of the lowest-lying (triplet and quintet) states of the KN molecule including the curve-crossing region is particularly challenging for electronic structure theory. All these facts prompted us to consider KN as a test problem to establish the applicability and potentiality of the IVO-SSMRPT method.

We can use the findings of Ishii *et al.*<sup>39</sup> as a reference to judge the performance of the IVO-SSMRPT method. To capture the full complexity of the problem, it is necessary to use sufficiently large basis sets. In our calculations, we have used the aug-cc-pVTZ basis for N and Sadlej's pVTZ basis for K (plus f-function).<sup>43</sup> We have calculated the PESs of the non-singlet states [with term symbols  $^3\Sigma^-$ ,  $^3\Pi$  and  $^5\Sigma^-$ ] including the curve-crossing region of the KN system generated *via* the IVO-SSMRPT method in order to assist experimental spectroscopic studies and radio-astronomical observations. Around the equilibrium region, all three states are well described respectively by the following electronic configurations (i)  $\{\text{core}\}(7\sigma)^2(8\sigma)^2(3\pi)^2$ , (ii)  $\{\text{core}\}(7\sigma)^2(8\sigma)^1(3\pi)^3$  and (iii)  $\{\text{core}\}(7\sigma)^2(8\sigma)^1(3\pi)^2(9\sigma)^1$ . But MR description is needed far from the equilibrium position. In our IVO-SSMRPT calculation, we have used CAS(6,6). Our results generated *via* the IVO-SSMRPT method are plotted in Fig. 13. The energy surfaces drawn in Fig. 13 also clearly illustrate that

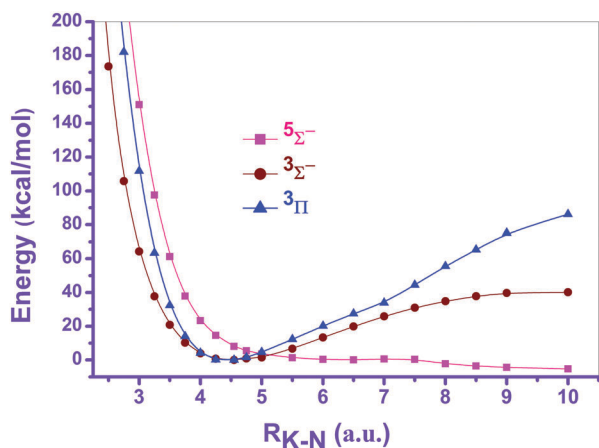


Fig. 13 Potential energy surfaces of experimentally unknown lowest lying non-singlet [ $^3\Sigma^-$ ,  $^3\Pi$  and  $^5\Sigma^-$ ] states of KN.

the topological behavior of dissociation of the surfaces is virtually identical with the state-of-the-art MRCI calculations [employing CASSCF as the reference function including all valence electrons and valence orbitals] of Ishii *et al.*<sup>39</sup> Similar to the computationally expensive MRCI+Q prediction, Fig. 13 clearly demonstrates that  $^3\Sigma^-$  is the electronic ground state of KN (similar to the NaN and LiN systems), although the energy gap with respect to the next (first) excited state  $^3\Pi$ , is very small. Note that although the energy term of the  $^3\Pi$  state is very small, 177.3  $\text{cm}^{-1}$ , the electronic ground state of KN has also been predicted as the  $^3\Sigma^-$  state by very high-level CASSCF-MRCI+Q calculations (where all valence electrons and valence orbitals were included in the active space of the CASSCF wave functions) according to Ishii *et al.*<sup>39</sup> It is also clear that the  $^3\Sigma^-$  and  $^3\Pi$  states provided by our IVO-SSMRPT/CAS(6,6) method are bound in nature similar to that of MRCI calculations.<sup>39</sup> In the dissociation limit, the  $^3\Sigma^-$  and  $^3\Pi$  states correlate with  $\text{K}(^2\text{S}) + \text{N}(^4\text{S})$  and  $\text{K}(^2\text{P}) + \text{N}(^4\text{S})$ . It would be interesting to note that around 2.440 Å (4.61 a.u.), the bound PESs of  $^3\Sigma^-$  and  $^3\Pi$  cross (real crossing) each other as per our IVO-SSMRPT calculations. The MRCI+Q<sup>39</sup> calculations show that these two energy surfaces cross at 2.422 Å (4.58 a.u.). We have noted an unphysical hump for the  $^3\Pi$  state at around 4.23 Å (8.00 a.u.). Ishii *et al.*<sup>39</sup> found a kink for this state at around 5.0 Å. According to the analysis of the electronic wave functions, the origin of this hump can be related to the avoided crossing in the  $^3\Pi$  state, in which the dominant configuration changes from  $\{\text{core}\}(7\sigma)^2(8\sigma)^1(3\pi)^3$  to the configuration of  $\{\text{core}\}(7\sigma)^2(8\sigma)^1(3\pi)^2(4\pi)^1$ . Although the CASSCF-MRCI+Q level of calculation supports the presence of a kink on the computed  $^3\Sigma^-$  surface, no noticeable kink appears in our IVO-SSMRPT calculations indicating that the mixing of the doubly excited configuration defined as  $\{\text{core}\}(7\sigma)^2(3\pi)^2(9\sigma)^2$  is not significant. Note that the presence of the kink will not affect the following estimations of spectroscopic constants in the respective electronic states as the kink(s) appears far from the equilibrium bond length.

In Table 8, we have tabulated the selected spectroscopic constants of this molecule employing Dunham's scheme to the computed PESs. Table shows that the performance of IVO-SSMRPT/CAS(6,6) is indeed very similar to that of the computationally laborious MRCI+Q. In MRCI+Q calculations, the equilibrium bond lengths,  $R_e$  (Å), for the  $^3\Sigma^-$  and  $^3\Pi$  states are 2.549 and 2.347, respectively, which are slightly longer and shorter than ours by 0.063 and 0.054, respectively. Our extracted harmonic frequencies,  $\omega_e$  ( $\text{cm}^{-1}$ ) for the  $^3\Sigma^-$  and  $^3\Pi$  states are slightly higher than the MRCI+Q calculated values by 53.7 and

Table 8 Selected spectroscopic constants [*viz.* equilibrium bond length  $R_e$  (Å), harmonic vibrational frequency  $\omega_e$  ( $\text{cm}^{-1}$ ), and dissociation energy  $D_e$  ( $\text{kcal mol}^{-1}$ )] of low-lying states of KN

State	Method	$R_e$	$\omega_e$	$D_e$
$^3\Sigma^-$	IVO-SSMRPT	2.486	378.1	30.11
	MRCI+Q <sup>39</sup>	2.549	324.4	19.32
$^3\Pi$	IVO-SSMRPT	2.401	421.4	64.16
	MRCI+Q <sup>39</sup>	2.347	394.0	54.68

27.4, respectively. Similar to MRCI estimates, the IVO-SSMRPT dissociation energy for the  $^3\Sigma^-$  and  $^3\Pi$  states is relatively small. Concerning the dissociation energy, the energies for the  $^3\Sigma^-$  and  $^3\Pi$  states are calculated as 30.11 and 64.16 kcal mol $^{-1}$ , respectively, which are larger than the values of MRCI+Q $^{39}$  indicating that IVO-SSMRPT provides much stronger bonds than those from MRCI+Q. Our estimated ground state dissociation energy is 30.11 kcal mol $^{-1}$ , which is almost the same as the value for the  $^3\Sigma^-$  NaP (28 kcal mol $^{-1}$ ). $^{77}$  The dissociation energy indicates that the bond in  $^3\Sigma^-$  KN is stronger than the one in  $^3\Sigma^-$  NaN (19.81 kcal mol $^{-1}$ ). $^{78}$  We hope that the IVO-SSMRPT/CAS(6,6) PESs and the spectroscopic parameters derived therefrom provide a reliable characterization of these non-singlet states similar to the MRCI+Q ones. The spectroscopic parameters assembled in the table await experimental investigations of KN, and we hope these results can assist in detecting the existence of KN in interstellar space.

#### D. Low-lying ionized states of water: ionization energies

For a more interesting study, we looked at the computation of ionization energies of water molecules. For this purpose we use a cc-pVTZ basis set in conjunction with CAS(6,6) [with six active electrons in six active orbitals ( $1b_1, 3a_1, 1b_2, 4a_1, 2b_2, 2b_1$ )] and do not correlate core electrons for  $C_{2v}$  H $_2$ O. The ground state,  $\tilde{X}^1A_1$  H $_2$ O has been extensively studied in the past. $^{79-82}$  There has been a great deal of interest in the ionization energies of H $_2$ O. $^{80,83-86}$  One must note that an accurate and balanced description of an ionized state calls for a truly reliable theoretical protocol. Ionized states possess a reasonable level of complexity owing to the involvement of two electronic states having different electron counts, with one state among them having a free radical character. Any theory that is being implemented to study such states should not only account for the electron correlation effects, but should also be capable of providing ample room to take care of the orbital relaxation and differential correlation effects that stem out from the loss of an electron to form the ionized state. In addition, since the terminal states are open-shell ground or excited states of the cation that have a diverse electronic structure, the theory must be able to judiciously treat the interplay of dynamical and non-dynamical electron correlation effects.

To evaluate the ionization energies, we have first optimized the ground state H $_2$ O along with the three lowest doublet states of ionized water (the ground electronic state of H $_2$ O $^+$ ,  $^2B_1$  and its two first excited states,  $^2A_1$  and  $^2B_2$ ). Bond parameters obtained by IVO-SSMRPT as well as other methods $^{79-82}$  for H $_2$ O are collected in Table 9. The results for different states

Table 9 Bond parameters of the ground state ( $\tilde{X}^1A_1$ ) water molecule obtained with different methods

Ref.	Methods/Basis	$R_e$ (Å)	$\angle$ H-O-H (°)
Present work	IVO-SSMRPT/cc-pVTZ	0.9636	103.8
	SSMRPT/cc-pVTZ	0.9625	104.1
79	CCSD(T)/cc-pVQZ	0.9579	104.12
81	3R-RMR-CCSD/cc-pVDZ	0.965	102.0
82	Experiment	0.95782	104.485

Table 10 Bond parameters of the oxoniumyl ion obtained with different methods for various doublet states

Ref.	State	Methods	$R_e$ (Å)	$\angle$ H-O-H (°)
Present work 80 88	$1^2B_1$	IVO-SSMRPT	1.000	108.2
		MRDCI	1.000	107.4
		Experiment	1.000	109.3
Present work	$1^2A_1$	IVO-SSMRPT	0.987	172.0
Present work 80	$1^2B_2$	IVO-SSMRPT	1.1421	57.1
		MRDCI	1.16	54.0

of H $_2$ O $^+$  are listed in Table 10. As seen from Tables 9 and 10, the IVO-SSMRPT method works well for the ionized species, as it does for other (neutral) molecules studied above.

The ground state geometry of H $_2$ O is reproduced well by the optimization scheme of IVO-SSMRPT. The IVO-SSMRPT and CCSD(T) $^{79}$  results show reasonable parallelism. For the equilibrium ground state geometry, the overall agreement of IVO-SSMRPT with experiments is within 0.006 Å and 0.7° for the OH bond length and  $\angle$  0.7°, respectively. Compared to experimental estimates, 3R-RMRCCSD [reduced multireference CCSD for three-dimensional model space] yields the equilibrium ground state geometry to within 0.007 Å in the OH bond length, while the HOH angle is accurate to 2.5°.

IVO-SSMRPT calculations suggest that the  $1^2B_1$  represents the ground state of the H $_2$ O $^+$ . It should be noted that the difference between the bond parameters of the ground state ( $1^2B_1$ ) of H $_2$ O $^+$  provided by SSSMRPT and MRDCI (multireference double excitation configuration interaction scheme) is very small. This doublet state according to IVO-SSMRPT optimization, has  $R_{OH} = 1.000$  Å at an angle HOH of 108.2° which deviates from experimental values by 0.0 Å and 1.1°, respectively. Photoelectronic spectroscopy $^{87}$  predicts the equilibrium geometry of  $1^2B_1$  H $_2$ O $^+$  to be  $\angle$  H-O-H = 110.46° and  $R_{O-H} = 0.9988$  Å, which bears a close proximity to our predictions.

At the level of IVO-SSMRPT calculations, the ionized state  $1^2A_1$  exhibits a minimum at  $R_{OH} = 0.987$  Å and  $\angle$  172.0°, indicating a nearly linear ( $D_{\infty h}$ ) nature of the state. One of the earlier theoretical study also supports the near linearity of  $1^2A_1$  H $_2$ O $^+$ . $^{80}$  The optimized geometry of H $_2$ O $^+$  is found by our calculations to be  $R_{OH} = 1.1421$  Å at 57.1° for the  $\angle$  HOH which is in good accord with the predictions of MRDCI calculations of Schneider *et al.* $^{80}$  On the basis of the molecular beam photoelectron findings, Reutt *et al.* $^{87}$  argued that the oxoniumyl ion in its first excited state,  $1^2A_1$  is almost linear, with OH bond distance  $R_{O-H} = 0.98$  Å, which is in close agreement with our estimates.

For a further test of the utility of the IVO-SSMRPT method, the results for the vertical ionization energies of H $_2$ O are compared with available experimental $^{88}$  and theoretical $^{80,83,85,86}$  data in Table 11. We have calculated the vertical ionization energies with the same basis set (cc-pVTZ) by estimating the energy differences of the three doublet states of H $_2$ O $^+$  with respect to the ground state of water at the computed optimized geometries. As seen in Table 11 the performance of the IVO-SSMRPT method for providing the ionization energies is very good. The minimum

**Table 11** Vertical ionization energies (eV) of H<sub>2</sub>O to different doublet states of H<sub>2</sub>O<sup>+</sup>

Ref.	State	Methods (eV)	IP
Present work 80 83 86	1 <sup>2</sup> B <sub>1</sub>	IVO-SSMRPT	12.45
		MRDCI	12.30
		CEPA	12.48
		IP-EOMCCSDT	11.81
		IP-EOMCCSDTQ	11.83
85 88		CASPT2	11.80
		Experiment	12.61
Present work 80 83 86	1 <sup>2</sup> A <sub>1</sub>	IVO-SSMRPT	14.88
		MRDCI	14.60
		CEPA	14.68
		IP-EOMCCSDT	13.83
		IP-EOMCCSDTQ	13.85
85 88		CASPT2	13.78
		Experiment	14.73
Present work 80 83 86	1 <sup>2</sup> B <sub>2</sub>	IVO-SSMRPT	18.05
		MRDCI	18.70
		CEPA	18.86
		IP-EOMCCSDT	18.59
		IP-EOMCCSDTQ	18.60
85 88		CASPT2	18.55
		Experiment	18.55

and maximum errors against experiments are 0.2 and 0.5 eV, respectively. The MRDCI scheme yields a similar level of accuracy for which the minimum and maximum errors are 0.1 and 0.3 eV, respectively. At this point it is worth mentioning that IVO-SSMRPT is explicitly size-extensive in contrast to the MRDCI scheme. For the IVO-SSMRPT and CASPT2 calculations, we observe that both provide the ionization energies of similar quality.<sup>85</sup> The CASPT2 underestimates the vertical ionization energies of H<sub>2</sub>O by 0.81 and 0.95 eV for 1<sup>2</sup>B<sub>1</sub> and 1<sup>2</sup>A<sub>1</sub>, respectively. For the 1<sup>2</sup>B<sub>2</sub> state, the CASPT2 result is in perfect agreement with the experimental finding. It is quite probable that this observation is a consequence of the (accidental) cancellation of errors, encountered quite often in the realm of electronic structure theory in a variety of contexts. Our estimates are also in good agreement with the data provided by the computationally expensive IP-EOMCC [EOMCC for ionization potential] calculations of Hirata *et al.*<sup>86</sup> (within 0.55–1.03 eV). Note that the error of IP-EOMCCSDTQ<sup>86</sup> against experimental estimates is between 0.05 and 0.88 eV. Thus, one can argue that the IVO-SSMRPT approach offers the flexibility to include the orbital relaxation, differential correlation, and additional correlation effects accompanying ionization on top of the ground state correlation components. Previous calculations of ΔCC [which obtain an ionization energy as a CC energy difference between the neutral species and cation]<sup>85</sup> and IP-EOMCC<sup>86</sup> methods clearly indicate that the proper treatment of the orbital relaxation effect is very crucial to get correct ionization energies for water. The results in the tables show that the SSMRPT with IVO-orbitals is quite dependable for the calculation of ionization energies, as would be expected from looking at the closeness of estimates with other reference results. Therefore, the IVO-SSMRPT approach is not only restricted to the treatment of the ground and excited state properties of spectroscopic interest but is also applicable to the low-lying ionized states.

By analyzing the components of reference orbitals, we argue that for the systems treated here the CASCI orbitals in the transition state or stretched bonds are noticeably delocalized compared to those in the reactant or equilibrium situation. Thus, our computations on these cases reveal that the accuracy of the IVO-SSMRPT method remains unaffected if the delocalization of orbitals of the reference wavefunction is significant. From the analysis it transpires that IVO-SSMRPT is a versatile *ab initio* method applicable to the ground, excited, and ionized states within a consistent theoretical framework.

## IV. General discussion

Despite its usefulness, there are several open problems in the IVO-SSMRPT method (similar to other widely used MRPT methods) that must be mentioned. Regardless of an unbiased treatment of all references, it is also worth noting the inability of the IVO-SSMRPT approach (like other Hilbert space based MR methods) to comply with the property of active-orbital invariance (originally attributed to the “proper residual” problem).<sup>89</sup> This issue appears to have noticeable numerical consequences for the SSMRPT method.<sup>2</sup> Despite the invariance of the zeroth order IVO-CASCI function, lack of invariance of the IVO-SSMRPT leads to size-consistency if the active orbitals are localized on different fragments (also shared by other JM-based MR methods). Another shortcoming of the IVO-SSMRPT method is the insufficient coupling between the virtual functions which can be maximum up to doubly excited with each other. Note that the virtual functions generated by the cluster operators acting on different reference functions are all decoupled for different reference functions which takes down the quality of the energies for more than two active electrons. The extent of deterioration of the results can be arrested by using localized orbitals.<sup>40</sup> Similar to other CAS based MR methods, IVO-SSMRPT has computational bottlenecks that prevent computations with large active spaces since the computational scaling of the method is proportional to the number of reference determinants. To avoid such limitations, several schemes have been proposed which allow the use of reference wave functions with large active spaces and arbitrary configuration selection.<sup>27–29,90</sup> In fact, much less research has been done to reduce the cost scaling for the MR-paradigm.<sup>91</sup> The computational and memory costs of the present method can be reduced by using an internally contracted (IC) scheme where the number of cluster amplitudes is no longer proportional to the number of reference configurations. With appropriate selection of the cluster operator, the method could be guaranteed to be orbital invariant within the IC framework. We are optimistic that the generality of the IVO-SSMRPT approach can be improved through a careful consideration of these issues.

In spite of the explicit intruder-free nature of the IVO-SSMRPT method, tiny humps can be observed of the order of a few kcal mol<sup>-1</sup> when computing error surfaces for methane with the 6-31G\* basis and ethane with the aug-ccpVTZ basis. A similar observation has also been reported in the context of other SSMR



methods in the recent past.<sup>92</sup> This unwanted kink has been ascribed to the small value of the reference coefficients which appear in the denominator of the cluster amplitude finding equation (*vide supra*). The kinks can be eliminated or at least attenuated by using the regularization scheme:<sup>93,94</sup>

$$\frac{1}{c_\mu^0} \rightarrow \frac{c_\mu^0}{(c_\mu^0)^2 + \omega^2}$$

where  $\omega$  is the damping parameter. We are

optimistic that the performance of the IVO-SSMRPT approach can be improved through the careful selection and optimization of  $\omega$ . The dropping of every  $c_\mu^0$  falling below a certain threshold in magnitude and zeroing the corresponding cluster amplitudes can eliminate most kinks in the PES as well. Jeszenski *et al.*<sup>94</sup> has argued that the redundancy due to spin-adaptation is also responsible for occasional kinks on PESs provided by the SSMRPT method. The expectation value form of IVO-SSMRPT:  $\langle E \rangle^2 = \sum_{\mu,\nu} c_\mu^0 \tilde{H}_{\mu\nu}^{(2)} c_\nu^0$  is free from this

effect; it however leaves the coefficients unrelaxed. The floating occupation molecular orbitals (FOMO)-based CASCI<sup>95</sup> method may be an attractive choice for covering the dominant part of the static electron correlation for performing SSMRPT computations for molecules that need a genuine MR description in a very economical, unbiased, and routine way and we plan to investigate this in the future.

Though our method is primarily designed to deal with the ground state, we have, nevertheless, implemented it to study a few low-lying excited states as well. This has only been possible owing to the structural flexibility of the method. A critical test of any single-root protocol is to describe the excited states with the same accuracy as for the ground state. There are certain issues that one faces while dealing with high-lying excited states of arbitrary symmetry with this method. A plausible explanation for this difficulty is as follows. To compute excited states of arbitrary space and spin symmetry, numerical problems related to the very small values of  $c_\mu$  are found to be prominent,<sup>94</sup> and it is often so extensive that one faces convergence failures. For all the excited states that we have computed, it has been envisaged that the convergence of the cluster finding equations are slower, as compared to that in the case of the ground state. Thus, dealing with such states, one might often need a greater number of iterations to “home” to the desired root while solving the IVO-SSMRPT equations. Moreover, orbital relaxation, the change of the differential correlations and the additional correlations accompanying excitation are very significant for the high-lying excited or ionized states and cannot be handled by a theory which is second-order perturbative in nature. For such situations explicit response based methods are needed. In the near future, we will try to formulate the SSMRPT-based linear response theory to compute the potential energy surfaces of excited states reached by arbitrary excitation manifolds. Additionally, the target state is not always energetically well-separated from the virtual functions in the case of computation of all types of excited states. Under such situations the method often feels threatened for the appearance of convergence problem.

## V. Conclusion

One of the most captivating challenges for the practitioners of quantum chemistry is to develop a formalism which can handle strongly correlated systems (and chemical situations/processes) affected by both dynamic correlation and static correlation in a faithful, correct and robust manner at an affordable computational cost. In order to meet this goal, we suggest the IVO-SSMRPT method (uses multideterminantal perturbations), which provides a second order perturbation estimate of the full CI energy, and typically features a separation of the electron correlation into a static and a dynamic contribution. It considers a CAS model space (to achieve the strict separability requirement), generated from a preliminary IVO-CASCI calculation. IVO-CASCI is well suited for capturing the multiconfigurational character of wave functions that is present during bond dissociation and at intersections between electronic states. Nevertheless, IVO-CASCI requires fewer parameters to describe the wave function than the conventional CASSCF. Our method is blessed with many important features (size-extensivity and intruder independence) of a good many-body method, making the approach very robust and reliable. We apply the IVO-SSMRPT method here to revisit the C–H, C–C, O–O, and C=C bond dissociations in methane, ethane, hydrogen peroxide, and ethene respectively. The energy surfaces for the lowest-lying states of the LiH and KN molecules have also been calculated by our method. We have also studied the photodissociation pathway of triplet ketene and the ionization energy of H<sub>2</sub>O. Besides bond dissociation, the method has also been used to predict barrier height. These systems are sufficiently complex for judging the ability and generality of the MR methods tailored to treat situations in which the diradical character changes significantly across the bond parameters.

The present results indicate that SSMRPT with CASSCF orbitals are good mimics of SSMRPT-corrected IVO-CASCI. An analysis of the total energies and error surfaces (nonparallelity errors) advocates that IVO-SSMRPT is reliable for both absolute and relative energies. We also note that IVO-SSMRPT provides results that are at least as accurate as other widely used MR-based methods. The quality of the results obtained from SSMRPT calculations remains almost unchanged even with drastic reductions in the computational cost during the construction of the zero-order wave-function. Note that the IVO-SSMRPT scheme possesses much better convergence characteristics than does the CASSCF-SSMRPT one, particularly when accessing excited and/or ionized states. The IVO-SSMRPT method provides very encouraging results at a fraction of the cost in both time as well as memory, and in many cases competitive with the much more resource-demanding current generation CC and MRCI level of calculations. One can achieve a correct and balanced description of both diradical and non-diradical natures of molecules, both at equilibrium and non-equilibrium structures with small active spaces. The overall agreement of our estimates with reference values illustrates that not only the ground state wavefunction but also the excited and the ionized states are well described by second order IVO-SSMRPT even with a simplified treatment of nondynamical correlation. It is to be pointed out that in spite of

its single root nature our methods works well even for the excited states of neutral and ionized species, since it has the ability to capture major differential correlation in conjunction with orbital relaxation effects on the top of other correlation effects during ionization and/or excitation. This fact bolsters our belief that IVO-SSMRPT protocol may be used with confidence for kinetics modelling of various reaction mechanisms and processes involving strongly correlated systems similar to other current generation CC and MR-based calculations.<sup>91</sup> Unfortunately, our results show that IVO-SSMRPT does not resolve the problem of a step-like structure near the dissociation threshold of triplet ketene like other previously published high-level theoretical studies. This situation cannot be changed after further advancement of the computation from SSMRPT approximation to the full-blown SSMRCC one. Therefore, simple high-level *ab initio* calculations will not be able to capture the essential aspects of the photo-dissociation mechanism of triplet ketene and hence it is still an unsolved problem despite a plethora of theoretical efforts. Finally, although IVO-SSMRPT application can be extended to other chemical systems of salient MR character, the method can be improved and refined for large-scale computations and for quantum chemical problems severely plagued by quasidegeneracy.

## Acknowledgements

The authors gratefully acknowledge the financial support of DST, India [Ref. No. EMR/2015/000124]. S. S. R., A. G., and A. S. thank the UGC (India), DST-Inspire (India) and CSIR (India), respectively for their research fellowships.

## References

- B. O. Roos, K. Andersson, M. P. Fülscher, P.-Å. Malmqvist, L. Serrano-Andrés, K. Pierloot and M. Merchán, *Adv. Chem. Phys.*, 1996, **93**, 219.
- S. Chattopadhyay, R. K. Chaudhuri, U. S. Mahapatra, A. Ghosh and S. Sinha Ray, *Wiley Interdiscip. Rev.: Comput. Mol. Sci.*, 2016, **6**, 266.
- K. Kowalski and P. Piecuch, *J. Chem. Phys.*, 2000, **113**, 18; K. Kowalski and P. Piecuch, *J. Chem. Phys.*, 2000, **113**, 5644; P. Piecuch, K. Kowalski, I. S. O. Pimentá and M. J. McGuire, *Int. Rev. Phys. Chem.*, 2002, **21**, 527; P. Piecuch and M. Włoch, *J. Chem. Phys.*, 2005, **123**, 224105; M. Włoch, M. D. Lodriguito, P. Piecuch and J. R. Gour, *Mol. Phys.*, 2006, **104**, 2149; M. Włoch, J. R. Gour and P. Piecuch, *J. Phys. Chem. A*, 2007, **111**, 11359; G. Fradelos, J. J. Lutz, T. A. Wesolowski, P. Piecuch and M. Włoch, *J. Chem. Theory Comput.*, 2011, **7**, 1647.
- A. I. Krylov, *Chem. Phys. Lett.*, 2001, **338**, 375; L. V. Slipchenko and A. I. Krylov, *J. Chem. Phys.*, 2005, **123**, 84107; A. I. Krylov, *Annu. Rev. Phys. Chem.*, 2008, **59**, 433; D. Casanova, L. V. Slipchenko, A. I. Krylov and M. Head-Gordon, *J. Chem. Phys.*, 2009, **130**, 044103.
- A. I. Krylov and C. D. Sherrill, *J. Chem. Phys.*, 2002, **116**, 3194; D. Casanova and M. Head-Gordon, *J. Chem. Phys.*, 2008, **129**, 064104.
- D. Kats and F. R. Manby, *J. Chem. Phys.*, 2013, **139**, 021102; D. Kats, *J. Chem. Phys.*, 2016, **144**, 044102.
- D. W. Small and M. Head-Gordon, *Phys. Chem. Chem. Phys.*, 2011, **13**, 19285; D. W. Small and M. Head-Gordon, *J. Chem. Phys.*, 2012, **137**, 114103; D. W. Small, K. V. Lawler and M. Head-Gordon, *J. Chem. Theory Comput.*, 2014, **10**, 2027; J. Lee, D. W. Small, E. Epifanovsky and M. Head-Gordon, *J. Chem. Theory Comput.*, 2017, **13**, 602.
- J. M. Wahlen-Strothman, T. M. Henderson, M. R. Hermes, M. Degroote, Y. Qiu, J. Zhao, J. Dukelsky and G. E. Scuseria, *J. Chem. Phys.*, 2017, **146**, 054110.
- K. Hirao, *Chem. Phys. Lett.*, 1992, **190**, 374; K. Hirao, *Int. J. Quantum Chem.*, 1992, **44**, 517.
- H. Nakano, *J. Chem. Phys.*, 1993, **99**, 7983.
- K. Andersson, P.-Å. Malmqvist, B. O. Roos, A. J. Sadlej and K. Wolinski, *J. Phys. Chem.*, 1990, **94**, 5483; K. Andersson, P. Å. Malmqvist and B. O. Roos, *J. Chem. Phys.*, 1992, **96**, 1218; P. Celani and H.-J. Werner, *J. Chem. Phys.*, 2000, **112**, 5546; P. Pulay, *Int. J. Quantum Chem.*, 2011, **111**, 3273.
- J. Finley, P.-A. Malmqvist, B. O. Roos and L. Serrano-Andres, *Chem. Phys. Lett.*, 1998, **288**, 299; T. Shiozaki, W. Györfly, P. Celani and H.-J. Werner, *J. Chem. Phys.*, 2011, **135**, 081106.
- C. Angeli, R. Cimiraglia, S. Evangelisti, T. Leininger and J.-P. Malrieu, *J. Chem. Phys.*, 2001, **114**, 10252; C. Angeli, R. Cimiraglia and J.-P. Malrieu, *J. Chem. Phys.*, 2002, **117**, 9138.
- C. Angeli, S. Borini, M. Cestari and R. Cimiraglia, *J. Chem. Phys.*, 2004, **121**, 4043.
- Z. Rolik, Á. Szabados and P. R. Surján, *J. Chem. Phys.*, 2003, **119**, 1922.
- Y. G. Khait, J. Song and M. R. Hoffmann, *J. Chem. Phys.*, 2002, **117**, 4133.
- U. S. Mahapatra, B. Datta and D. Mukherjee, *J. Phys. Chem. A*, 1999, **103**, 1822; F. A. Evangelista, A. C. Simmonett, H. F. Schaefer III, D. Mukherjee and W. D. Allen, *Phys. Chem. Chem. Phys.*, 2009, **11**, 4728; S. Mao, L. Cheng, W. Liu and D. Mukherjee, *J. Chem. Phys.*, 2012, **136**, 024106.
- U. S. Mahapatra, S. Chattopadhyay and R. K. Chaudhuri, *J. Chem. Phys.*, 2008, **129**, 024108; U. S. Mahapatra, S. Chattopadhyay and R. K. Chaudhuri, *J. Chem. Phys.*, 2009, **130**, 014101; U. S. Mahapatra, S. Chattopadhyay and R. K. Chaudhuri, *J. Phys. Chem. A*, 2010, **114**, 3668; U. S. Mahapatra, S. Chattopadhyay and R. K. Chaudhuri, *J. Chem. Theory Comput.*, 2010, **6**, 662.
- E. Xu, D. Zhao and S. Li, *J. Chem. Theory Comput.*, 2015, **11**, 4634.
- Y. K. Choe, Y. Nakao and K. Hirao, *J. Chem. Phys.*, 2001, **115**, 621; Y. Nakao, Y.-K. Choe, K. Nakayama and K. Hirao, *Mol. Phys.*, 2002, **100**, 729.
- D. Robinson and J. J. W. McDouall, *Mol. Phys.*, 2006, **104**, 681; D. Robinson and J. J. W. McDouall, *J. Chem. Theory Comput.*, 2007, **3**, 1306.
- S. Grimme and M. Waletzke, *Phys. Chem. Chem. Phys.*, 2000, **2**, 2075.

- 23 R. K. Chaudhuri, K. F. Freed, S. Chattopadhyay and U. S. Mahapatra, *J. Chem. Phys.*, 2008, **128**, 144304; S. Chattopadhyay, R. K. Chaudhuri and U. S. Mahapatra, *Phys. Chem. Chem. Phys.*, 2011, **13**, 7514.
- 24 L. Roskop and M. S. Gordon, *J. Chem. Phys.*, 2011, **135**, 044101.
- 25 P. R. Surján, I. Mayer and I. Lukovits, *Phys. Rev. A: At., Mol., Opt. Phys.*, 1985, **32**, 748; M. Kobayashi, Á. Szabados, H. Nakai and P. R. Surján, *J. Chem. Theory Comput.*, 2010, **6**, 2024; P. Jeszenszki, P. R. Surján and Á. Szabados, *J. Chem. Phys.*, 2013, **138**, 124110.
- 26 D. Casanova and M. Head-Gordon, *Phys. Chem. Chem. Phys.*, 2009, **11**, 9779; F. Bell, P. M. Zimmerman, D. Casanova, M. Goldey and M. Head-Gordon, *Phys. Chem. Chem. Phys.*, 2012, **15**, 358; P. M. Zimmerman, F. Bell, M. Goldey, A. T. Bell and M. Head-Gordon, *J. Chem. Phys.*, 2012, **137**, 164110; N. J. Mayhall, M. Goldey and M. Head-Gordon, *J. Chem. Theory Comput.*, 2014, **10**, 589.
- 27 Y. Kurashige and T. Yanai, *J. Chem. Phys.*, 2013, **135**, 094104; S. Sharma and G. K.-L. Chan, *J. Chem. Phys.*, 2014, **141**, 111101; E. Xu, D. Zhao and S. Li, *J. Chem. Theory Comput.*, 2015, **11**, 4634.
- 28 Y. Kurashige, J. Chalupský, T. N. Lan and T. Yanai, *J. Chem. Phys.*, 2014, **141**, 174111; C. Li and F. A. Evangelista, *J. Chem. Theory Comput.*, 2015, **11**, 2097; K. P. Hannon, C. Li and F. A. Evangelista, *J. Chem. Phys.*, 2016, **144**, 204111.
- 29 C. Angeli, C. J. Calzado, R. Cimiraglia and J.-P. Malrieu, *J. Chem. Phys.*, 2006, **124**, 234109.
- 30 S. Chattopadhyay, R. K. Chaudhuri and U. S. Mahapatra, *J. Comput. Chem.*, 2015, **36**, 907; S. Sinha Ray, A. Ghosh, S. Chattopadhyay and R. K. Chaudhuri, *J. Phys. Chem. A*, 2016, **120**, 5897; S. Sinha Ray, P. Ghosh, R. K. Chaudhuri and S. Chattopadhyay, *J. Chem. Phys.*, 2017, **146**, 064111.
- 31 J. Segarra-Martí, M. Garavelli and F. Aquilante, *J. Chem. Theory Comput.*, 2015, **11**, 3772.
- 32 S. Chattopadhyay and R. K. Chaudhuri, *Many-Body Methods for Atoms and Molecules*, CRC-press, USA, 2016.
- 33 B. O. Roos, P. R. Taylor and P. E. M. Siegbahn, *Chem. Phys.*, 1980, **48**, 157; M. W. Schmidt and M. S. Gordon, *Annu. Rev. Phys. Chem.*, 1998, **49**, 233; B. G. Levine and T. J. Martínez, *Annu. Rev. Phys. Chem.*, 2007, **58**, 613.
- 34 G. Hose and U. Kaldor, *J. Phys. B: At., Mol. Opt. Phys.*, 1979, **12**, 3827; K. Kowalski and P. Piecuch, *Phys. Rev. A: At., Mol., Opt. Phys.*, 2000, **61**, 052506.
- 35 D. M. Potts, C. M. Taylor, R. K. Chaudhuri and K. F. Freed, *J. Chem. Phys.*, 2001, **114**, 2592; S. Chattopadhyay, R. K. Chaudhuri and K. F. Freed, *J. Phys. Chem. A*, 2011, **115**, 3665.
- 36 B. O. Roos and K. Andersson, *Chem. Phys. Lett.*, 1995, **245**, 215; Y.-K. Choe, H. A. Witek, J. P. Finley and K. Hirao, *J. Chem. Phys.*, 2001, **114**, 3913.
- 37 S.-W. Chang and H. A. Witek, *J. Chem. Theory Comput.*, 2012, **8**, 4053.
- 38 J. M. Rintelman, I. Adamovic, S. Varganov and M. S. Gordon, *J. Chem. Phys.*, 2005, **122**, 044105; Z. Azizi, B. O. Roos and V. Veryazova, *Phys. Chem. Chem. Phys.*, 2006, **8**, 2727.
- 39 K. Ishii, T. Taketsugu and K. Yamashita, *J. Chem. Phys.*, 2007, **127**, 194307.
- 40 U. S. Mahapatra, B. Datta and D. Mukherjee, *Mol. Phys.*, 1998, **94**, 157; F. A. Evangelista, E. Prochnow, J. Gauss and H. F. Schaefer, *J. Chem. Phys.*, 2010, **132**, 074107; S. Das, D. Mukherjee and M. Kállay, *J. Chem. Phys.*, 2010, **132**, 074103.
- 41 K. G. Dyall, *J. Chem. Phys.*, 1995, **102**, 4909.
- 42 M. W. Schmidt, K. K. Baldrige, J. A. Boatz, S. T. Elbert, M. S. Gordon, J. H. Jensen, S. Koseki, N. Matsunaga, K. A. Nguyen, S. Su, T. L. Windus, M. Dupuis and J. A. Montgomery, Jr., *J. Comput. Chem.*, 1993, **14**, 1347.
- 43 D. Feller, *J. Comput. Chem.*, 1996, **17**, 1571; K. L. Schuchardt, B. T. Didier, T. Elsethagen, L. Sun, V. Gurumoorthi, J. Chase, J. Li and T. L. Windus, *J. Chem. Inf. Model.*, 2007, **47**, 1045 see also [www.emsl.pnl.gov/forms/basisform.html](http://www.emsl.pnl.gov/forms/basisform.html).
- 44 F. B. Brown and D. G. Truhlar, *Chem. Phys. Lett.*, 1985, **113**, 441.
- 45 A. Dutta and C. D. Sherrill, *J. Chem. Phys.*, 2003, **118**, 1610; M. L. Abrams and C. D. Sherrill, *J. Phys. Chem. A*, 2003, **107**, 5611.
- 46 A. Golubeva, A. V. Nemukhin, L. Harding, S. J. Klippenstein and A. I. Krylov, *J. Phys. Chem. A*, 2007, **111**, 13264.
- 47 A. Azenkeng, Y. G. Khait and M. R. Hoffmann, *Mol. Phys.*, 2007, **105**, 2819.
- 48 U. Bozkaya and H. F. Schaefer III, *J. Chem. Phys.*, 2012, **136**, 204114.
- 49 J. P. Coe, D. J. Taylor and M. J. Paterson, *J. Chem. Phys.*, 2012, **137**, 194111.
- 50 F. Chen and Z. Fan, *J. Comput. Chem.*, 2014, **35**, 121.
- 51 D. L. Gray and A. G. Robiette, *Mol. Phys.*, 1979, **37**, 1901.
- 52 R. J. Duchovic, W. L. Hase, H. B. Schlegel, M. J. Frisch and K. Raghavachari, *Chem. Phys. Lett.*, 1982, **89**, 120; C. Sosa, J. Noga, G. D. Purvis III and R. J. Bartlett, *Chem. Phys. Lett.*, 1988, **153**, 139.
- 53 P. U. Manohar and A. I. Krylov, *J. Chem. Phys.*, 2008, **129**, 194105.
- 54 M. Musiał, S. A. Kucharski and R. J. Bartlett, *J. Chem. Theory Comput.*, 2011, **7**, 3088.
- 55 K. R. Yang, A. Jalan, W. H. Green and D. G. Truhlar, *J. Chem. Theory Comput.*, 2013, **9**, 418.
- 56 S. Hirata, P. D. Fan, A. A. Auer, M. Nooijen and P. Piecuch, *J. Chem. Phys.*, 2004, **121**, 12197.
- 57 See <http://physics.nist.gov/PhysRef Data/> for information about experimental values.
- 58 B. Kuhn, T. R. Rizzo, D. Luckhaus, M. Quack and M. A. Suhm, *J. Chem. Phys.*, 1999, **111**, 2565.
- 59 K. Ruedenberg, L. M. Cheung and S. T. Elbert, *Int. J. Quantum Chem.*, 1979, **16**, 1069.
- 60 M. L. Abrams and C. D. Sherrill, *Chem. Phys. Lett.*, 2004, **395**, 227.
- 61 R. J. Bartlett and M. Musiał, *J. Chem. Phys.*, 2006, **125**, 204105.
- 62 E. R. Lovejoy, S. K. Kim and C. B. Moore, *Science*, 1992, **256**, 1541; S. K. Kim, E. R. Lovejoy and C. B. Moore, *J. Chem. Phys.*, 1995, **102**, 3202.
- 63 E. R. Lovejoy, S. K. Kim and C. B. Moore, *Science*, 1992, **256**, 1541; S. K. Kim, E. R. Lovejoy and C. B. Moore, *J. Chem. Phys.*, 1995, **102**, 3202.

- 64 R. A. King, W. D. Allen, B. Ma and H. F. Schaefer III, *Faraday Discuss.*, 1998, **110**, 23.
- 65 J. G. Gezelter and W. H. Miller, *J. Chem. Phys.*, 1996, **104**, 3546.
- 66 J. E. Subotnik, A. Sodt and M. Head-Gordon, *J. Chem. Phys.*, 2006, **125**, 074116.
- 67 R. K. Chaudhuri and S. L. N. G. Krishnamachari, *J. Phys. Chem. A*, 2008, **112**, 4399.
- 68 Q. Cui and K. Morokuma, *J. Chem. Phys.*, 1997, **107**, 4951; A. L. Kaledin and K. J. Seong, *J. Phys. Chem. A*, 2001, **105**, 2731.
- 69 Y. Ogihara, T. Yamamoto and S. Kato, *J. Phys. Chem. A*, 2010, **114**, 9981; Y. Ogihara, T. Yamamoto and S. Kato, *Chem. Phys. Lett.*, 2011, **511**, 28; Y. Ogihara, T. Yamamoto and S. Kato, *J. Chem. Theory Comput.*, 2011, **7**, 2507.
- 70 G. Leu, C. Huang, S. Lee, Y. Lee and I. Chen, *J. Chem. Phys.*, 1998, **109**, 9340; R. A. King, W. D. Allen and H. F. Schaefer III, *J. Chem. Phys.*, 2000, **112**, 5585.
- 71 S. Ben-Shlomo and U. Kaldor, *J. Chem. Phys.*, 1988, **89**, 956.
- 72 G. E. Scuseria, T. P. Hamilton and H. F. Schaefer III, *J. Chem. Phys.*, 1990, **92**, 568; W. Cencek and J. Rychlewski, *Chem. Phys. Lett.*, 2000, **320**, 549; W.-C. Tung, M. Pavanello and L. Adamowicz, *J. Chem. Phys.*, 2011, **134**, 064117.
- 73 P. Tecmer, K. Boguslawski, P. A. Johnson, P. A. Limacher, M. Chan, T. Verstraelen and P. W. Ayer, *J. Phys. Chem. A*, 2014, **118**, 9058.
- 74 X. Li and J. Paldus, *J. Chem. Phys.*, 2003, **119**, 5346.
- 75 P. K. Tamukong, Y. G. Khait and M. R. Hoffmann, *J. Phys. Chem. A*, 2017, **121**, 256.
- 76 Y. C. Chan, D. R. Harding, W. C. Stwalley and C. R. Vidal, *J. Chem. Phys.*, 1986, **85**, 2436; W. C. Stwalley and W. T. Zemke, *J. Phys. Chem. Ref. Data*, 1993, **22**, 87.
- 77 D. Tzeli, A. Papakondylis and A. Mavridis, *THEOCHEM*, 1997, **417**, 277.
- 78 K. Ishii, T. Taketsugu and K. Yamashita, *Chem. Phys. Lett.*, 2006, **427**, 1.
- 79 J. M. L. Martin, *Chem. Phys. Lett.*, 1995, **242**, 343.
- 80 F. Schneider, F. Di Giacomo and F. A. Gianturco, *J. Chem. Phys.*, 1996, **105**, 7560.
- 81 X. Li and J. Paldus, *J. Chem. Phys.*, 1999, **110**, 2844.
- 82 R. A. Mc Clatchey, W. S. Benedict, S. A. Clough, D. E. Burch and R. F. Calfee, in *AFCRL Atmospheric absorption line parameters compilation, Air force Cambridge research laboratories*, ed. L. G. Hanscom Field, Bedford, Massachusetts, 1973; O. L. Polyansky, A. G. Császár, S. V. Shirin, N. F. Zobov, P. Bartletta, J. Tennyson, D. W. Schwenke and P. J. Knowles, *Science*, 2003, **299**, 539–542; A. G. Császár, G. Czakó, T. Furtenbacher, J. Tennyson, V. Szalay, S. V. Shirin, N. F. Zobov and O. L. Polyansky, *J. Chem. Phys.*, 2005, **122**, 214305.
- 83 W. Meyer, *Int. J. Quantum Chem.*, 1971, **5**, 341.
- 84 B. Das and J. W. Farley, *J. Chem. Phys.*, 1991, **95**, 8809; M. Staikova, B. Engels, M. Peric and S. D. Peyerimhoff, *Mol. Phys.*, 1993, **80**, 1485.
- 85 J. Olsen, P. Jørgensen, H. Koch, A. Balkova and R. J. Bartlett, *J. Chem. Phys.*, 1996, **104**, 8007.
- 86 S. Hirata, P.-D. Fan, A. A. Auer, M. Nooijen and P. Piecuch, *J. Chem. Phys.*, 2004, **121**, 12197; M. Kamiya and S. Hirata, *J. Chem. Phys.*, 2006, **125**, 074111.
- 87 J. E. Reutt, L. S. Wang, Y. T. Lee and D. A. Shirley, *J. Chem. Phys.*, 1986, **85**, 6928.
- 88 C. R. Brundle and D. W. Turner, *Proc. R. Soc. London, Ser. A*, 1968, **307**, 27.
- 89 L. Kong, *Int. J. Quantum Chem.*, 2009, **109**, 441; A. Sen, S. Sen and D. Mukherjee, *J. Chem. Theory Comput.*, 2015, **11**, 4129.
- 90 F. Menezes, D. Kats and H.-J. Werner, *J. Chem. Phys.*, 2016, **145**, 124115.
- 91 S. J. Klippenstein, V. S. Pande and D. G. Truhlar, *J. Am. Chem. Soc.*, 2014, **136**, 528.
- 92 A. Engels-Putzka and M. Hanrath, *Mol. Phys.*, 2009, **107**, 143; S. Das, D. Mukherjee and M. Kállay, *J. Chem. Phys.*, 2010, **132**, 074103.
- 93 P. C. Hansen, *Rank-Deficient and Discrete Ill-Posed Problems: Numerical Aspects of Linear Inversion*, SIAM Monographs on Mathematical Modeling and Computation, Society for Industrial and Applied Mathematics, Philadelphia, PA, 1998.
- 94 Á. Szabados, *J. Chem. Phys.*, 2011, **134**, 174113; P. Jeszenszki, P. R. Surján and Á. Szabados, *J. Chem. Phys.*, 2013, **138**, 124110.
- 95 G. Granucci and A. Toniolo, *Chem. Phys. Lett.*, 2000, **325**, 79; P. Slavček and T. J. Martinez, *J. Chem. Phys.*, 2010, **132**, 234102.